*Internet Electronic Conference of Molecular Design* **2003**, November 23 – December 6
**BioChem** Press http://www.biochempress.com

# Avoided Curves Crossings of the Rydberg $[(AH_a^+)(e^-)_{Rydberg}]$ (a=2-4) Radical

Jong Keun Park

Department of Chemistry and Central Laboratory, Pusan National University, Pusan 609-735, Korea

## Abstract

Potential energy curves of the ground and low lying excited states for the dissociation of the Rydberg $AH_a$ ($NH_4$, $H_3O$, $H_2F$; 11 electron species) radical into $[AH_b + H_c$ ; b=1-3, c=1-2, b+c=a] have been calculated using ab initio Hartree-Fock (HF) and singly and doubly excited configuration interaction (SDCI) methods with a large basis set including Rydberg basis functions. In the ground and excited correlation curves, the potential curves of the $[(AH_a^+)(e^-)_{Rydberg}]$ radical diabatically correlate to the $[AH_b$ (n→3s, 3p) + $H_c]$ and the $[AH_b^+ + H_c^-]$ asymptotes. At shorter than $R_{(AH)} \cong 2.0$ Å, the avoided curve crossings between the dissociative diabatic states of the $[(AH_a^+)(e^-)_{Rydberg}]$ radical and the repulsive diabatic states emerging from the antibonding interactions of the $[AH_b$ (n→3s, 3p) + $H_c]$ asymptotes are found mainly. While, at larger than $R_{(AH)} \cong 2.0$ Å, the avoided curve crossings between the attractive diabatic states emerging from a bonding interaction of the $[AH_b^+ + H_c^-]$ asymptotes and the repulsive diabatic states from the antibonding orbitals of its asymptotes are found. A maximum position of the potential energy barrier of the ground correlation curve is located out of line of those of the excited states. The potential energy barriers formed by some avoided curve crossings are found to be relatively low. The potential wells are shallowly quasibound. The potential energy gaps between the Rydberg $AH_a$ radical and its dissociation asymptotes are very low. The relative stabilities of metastable states from $NH_4$ to $H_2F$ are decrease monotonously.

# 1 INTRODUCTION

Recently, the photodissociation reactions of the Rydberg $[(AH_a^+)(e^-)_{Rydberg}]$ radical have been one of the issues as a fundamental unit in photochemical processes of $(AH_{a-1})_n$ clusters.[1-64] Since the $[(AH_a^+)(e^-)_{Rydberg}]$ radical has a short lifetime and a low energy barrier relative to the corresponding dissociative products $[(AH_{a-1} + H), (AH_{a-2} + H_2)]$, the stabilities and electronic structures of $AH_a$ have been widely characterized by experimental[1-19,33-42,63,64] and theoretical[20-32,43-62] methods. The $AH_a$ radical in clusters has been known to be stabilized by the complexation with its neutral molecule species,[1-19,33-42] For example, the lifetime of the $NH_4$ radical in ammonia clusters[1-7] was observed to be $10^6$ times longer than that of the monomer. The lifetime of $NH_4$ is shorter than 1 μs, while those of $ND_4$ and $NT_4$ are longer than 10 μs. $NH_4$ relative to its dissociation products is unstable by 1.1 kcal/mol, while $ND_4$ and $NT_4$ are stable by 0.5-1.2 kcal/mol. Because of the slightly high dissociation barriers of the isotopic species ($ND_4$, $NT_4$), the stabilities of these species in stead of $NH_4$ have been studied extensively.[8-19] The stability and existence of the Rydberg $H_3O$ radical have been one of the topics in the quantum dynamics and energetics of $(H_2O)_n$ clusters.[33-51] The Rydberg $(H_3O^+)(e^-)_{3s}$ radical can be stabilized by the complexation with water species like a Rydberg $(NH_4^+)(e^-)_{3s}$ radical.

Since the stabilities and Rydberg transitions of $NH_4$ firstly suggested by Schuster[8] and Schüler *et al.*,[9] the existence of the $NH_4$ radical have been characterized by various theoretical methods.[20-32] According to the potential energy curves of $NH_4$ constructed by Kassab and Evleth,[21.22] the stability and electronic structure of $NH_4$ depend on its structural correlation with the first Rydberg excited state emerging from ($NH_3$ + H) and ($NH_2$ + $H_2$). The potential energy barrier of the state is made from the avoided curve crossing between the dissociative state of $(NH_4^+)(e^-)_{3s}$ and the repulsive state emerging from ($NH_3$ + H) and ($NH_2$ + $H_2$). The potential barriers and dissociation products are found to be high by some electron volts. By the potential energy curves of Kaspar *et al.*,[23] the relative stability and the dissociation barrier were depended by the electron correlation. At the UHF level, the dissociations of $NH_4$ into ($NH_3$ + H) or ($NH_2$ + $H_2$) are both exothermic, while, at the SDCI level, the dissociations are endothermic. According to the potential energy curves of Cardy *et al.*,[25] the formation reaction of $NH_4$ from ($NH_2$ + $H_2$) is slightly exothermic, whereas the reaction from ($NH_3$ + H) is endothermic. By the above results, the lifetime of $NH_4$ is essentially depended on the height of the potential energy barrier for the dissociation of $NH_4$ into its asymptotes.

Since the existence of $H_3O$ based on thermodynamic cycles are firstly suggested by Bernstein,[33] the stabilities of the Rydberg $H_3O$ radical have been performed by various experimental techniques.[34-42] By indirect kinetic studies, the existence of $H_3O$ as an intermediate (a lifetime of $\cong 10^{-10}$ sec) of the radiolysis of water was reported by Magee,[34] Sworski,[35] and Kongshang *et al.*[36] Using mass spectrometer equipped with two different reactors designed to produce reactive species, Melton and Joy[37] detected the existence of the $H_3O$ species produced by irradiating water vapor with ionizing electron. Martin and Swift[38] claimed to have obtained the ESR spectrum of $H_3O$. Gellene and Porter[40] generated the oxonium $H_3O$ radical by neutralizing a fast beam of ions in the near resonant electron transfer reaction. But, some workers could not obtain any experimental results for the existence of $H_3O$. In the collisions of beam of H and $H_2O$ conducted by Bassi *et al.*,[42] any evidence for a bound state in the relative velocity range of $\cong 10^{-5}$ (cm/sec) was not investigated. In ion-beam study performed by Williams and Porter,[10] a metastable state of $H_3O$ with a lifetime greater than $10^{-7}$ sec was not obtained.

The stabilities of $H_3O$ and the ground potential energy curve of the dissociation of $H_3O$ into ($H_2O$ + H) or (OH + $H_2$) have been theoretically investigated by some groups.[37,43-51] Melton and Joy,[37] Bishop,[43] and Schwarz[50] groups suggested that the stability of $H_3O$ would be stable or metastable relative to its asymptotes. According to their curves investigated by Gangi and Bader,[44] Niblaeus *et al.*,[46] and Luo and Jungen,[49] the ground $^2A_1$ state surface along the OH bond rupture has a very low energy barrier and the curve is quasibound state. Gangi and Bader studied the ground potential energy curve for the dissociation reaction of $H_3O$ into ($H_2O$ + H) using the UHF method. At $R_{(OH)} \cong 1.21$ Å, the energy barrier of the dissociation reactions is found to be ≅0.29 eV. The dissociation energy and vertical ionization energy are ≅1.22 and ≅5.36 eV, respectively. Using an UHF-CI method, the energy surface of $H_3O$ is performed by Niblaeus *et al.* At $R_{(OH)} \cong 1.248$ Å, the potential barrier is found to be ≅0.13 eV. The energy gap between $H_3O$ and ($H_2O$ + H) is ≅0.89 eV. In the various possible dissociation paths of $H_3O$ into ($H_2O$ + H) investigated by Luo and Jungen, the ground potential energy curve ($^2A_1$) along the OH bond rupture has a very low barrier of ≅0.08 eV. The curve is quasibound state. At $R_{(OH)} \cong 2.5$ Å, the curve is also bound shallowly. But, Lathan *et al.*[45] claimed that $H_3O$ would be unstable with respective to its asymptotes. They concluded that the origin of the barrier is an avoided curve crossing between a repulsive state and an attractive Rydberg state. The barrier height of the curve is investigated to be relatively low. And the formation reaction of $AH_a$ from its dissociation products are isoenergetic or very slightly endothermic.[20-32,43-51] But, the avoided curve crossings have not been represented clearly.

The stabilities and electronic structures of $H_2F$ with bent or linear geometry have been studied with the various theoretical[52-62] and experimental[63,64] methods. $H_2F$ with 11 electron systems is isoelectronic structure with $NH_4$ and $H_3O$, which are observed in the metastable states. By a combination of neutralized ion beam and charge stripping techniques,[63] an experimental evidence for metastable state of $D_2F$ is observed by Raksit *et al.* The lifetime of the metastable state is greater than 0.4 μs. But, the metastable states of HDF or $H_2F$ are not observed. Using the MRD-CI method, the ground and few excited states of $H_2F$ were calculated by Petsalakis *et al.*[58] These states are bound and have potential minima at geomteries similar to that of the cation $H_2F^+$. Until now, except for the result of Petsalakis *et al.*, the metastable state of $H_2F$ have not been found.[52-57,59-64]

Although the stabilities and geometric structures of $[(AH_a^+)(e^-)_{Rydberg}]$ in the hydrated and neutral molecule clusters have been studied with the various methods, the investigation of the potential energy curves for the dissociation of $[(AH_a^+)(e^-)_{Rydberg}]$ into ($AH_b$ + $H_c$) seems to be worth carrying out on the basis of the following points. (i) How are relative potential barriers of the potential energy curves for dissociation reactions from $NH_4$ to $H_2F$? (ii) On the ground and low lying excited curves, a maximum position is represented between $R_{(AH)} \cong 1.5$ and 2.5 Å, while, on the highly excited curves, two maximum positions are represented. What kinds of avoided curve crossings are occurred on the dissociation reactions? (iii) Why is the maximum position made by the avoided curve crossing located near the equilibrium geometry ($R_{(AH)} \cong 1.59$ and 1.40 Å)? (iv) Is the barrier height of the ground potential curve found to be low or high? (v) Is the dissociation reaction of $AH_a$ into ($AH_b$ + $H_c$) endothermic or exothermic? (vi) The potential energy barriers of the potential curves for the dissociation reaction of $AH_a$ into ($AH_b$ + $H_c$) are not yet investigated clearly. Are the energy barriers of the potential curves made by the avoided curve crossing? To answer above questions, we have studied the state-to-state correlation curves for $AH_a$ dissociating into ($AH_b$ + $H_c$) in order to investigate the stabilities and avoided crossings. Our correlation curves give the detailed informations of the crossing positions and barrier heights for $AH_a$ dissociating into ($AH_b$ + $H_c$).

## 2 Computational Method

The basis sets chosen are the triple zeta basis on N (521/2111),[65] O (5311111/32111),[66] and H(511).[67] Two extra d type polarization functions are added to nitrogen ($\alpha_d$=0.412, 1.986)[65] and oxygen ($\alpha_d$=2.22, 0.874).[68] One extra p type function to hydrogen ($\alpha_p$=0.990495).[65] The diffuse

Rydberg basis functions are additionally augmented on nitrogen ($\alpha_s$=0.028, 0.0066; $\alpha_p$=0.025, 0.0051; $\alpha_d$=0.015, 0.0032)[69] and oxygen ($\alpha_s$=0.008, 0.032; $\alpha_p$=0.051, 0.02; $\alpha_d$=0.345, 0.143)[68] to describe the Rydberg states of $NH_2$, $NH_3$, $NH_4$, $H_2O$, and $H_3O$.

To draw the potential energy curves, we have used the characteristics of the states twofold. For the dissociation of $AH_a$ into its dissociation products, the molecular orbital and geometric structure at each internuclear distance are calculated with the restricted open shell Hartree-Fock method (ROHF). And the molecular orbital and optimized structure were used as input for subsequent the singly and doubly excited configuration interaction (SDCI) calculation. That is, the molecular orbital for a configuration interaction (CI) is determined with ROHF's result. The singly and doubly excited configuration interaction method is used for the potential energy calculation with the GAMESS package. By changing the internuclear distance, the whole procedure has been repeated from $AH_a$ to its dissociation products. The internuclear distances [$R_{(AH)}$] range are from 0.9 to 14.0 Å. The SDCIs for the neutral ($H_2$, $NH_2$, $NH_3$, $NH_4$, OH, $H_2O$, and $H_3O$) and ionic species ($H^-$, $H_2^-$, $NH_2^+$, $NH_3^+$, $OH^+$, $H_2O^+$, and $H_3O^+$) are also performed separately.

All geometric structures for the ground states of $H_2$, $NH_2$, $NH_3$, $NH_4$, OH, $H_2O$, $H_3O$, and its cations are fully optimized with the Hartree-Fock (HF), second-order Möller-Plesset (MP2), and coupled cluster with both single and double substitution [CCSD(t)] levels using GAUSSIAN 98. The excited states of $NH_4$ and $H_3O$ are somewhat of a Rydberg nature with a cationic core. Therefore, the geometric structures of these states are expected to be similar to those of the corresponding cations. To examine the appropriateness of the procedure, the potential energy of the ground state surface from $AH_a$ to its dissociation products has been calculated with the SDCI and CCSD(t) methods. Meanwhile, to obtain the metastable state of the Rydberg $H_2F$ radical, the geometric structures are optimized using the basis set cited from the Reference 58. But, the optimized structure of $H_2F$ could not obtain.

## 3 RESULTS AND DISCUSSION

### 3.1 Potential Curves of $NH_4$ Dissociating into its Asymptotes

The bond lengths at the equilibrium and transition states and the relative energies of the $NH_4$ radical dissociating into ($NH_3$ + H) and ($NH_2$ + $H_2$) are listed in Table I together with the ionization and excitation energies of $NH_4$, $NH_3$, and $NH_2$. Our results for the ammonia molecules [$NH_n$ (n=2-4)] calculated by SDCI and CCSD(t) are in reasonable agreement with the experimental[1-19,70,75] and theoretical[20-32,71-74,76-81] values. Since the ground state of $NH_4$ has an electron in a Rydberg 3s orbital, $NH_4$ itself is often called the Rydberg radical and $NH_4$ is a semi-ionic state. At the equilibuium geometry of $NH_4$, $R_{(NH)eq}$≅1.04 Å is slightly larger than those [$R_{(NH)eq}$≅1.01 Å] of $NH_3$. For $NH_4$ dissociating into ($NH_3$ + H), the bond lengths [$R_{(NH)TS}$] at the transition state is ≅1.439 Å. The energy barrier heights of $^2A_1$ from the transition state to $NH_4$ and ($NH_3$ + H) are ≅0.83 and 0.61 eV, respectively. The energy gap between $NH_4$ and ($NH_3$ + H) is -0.22 eV. For $NH_4$ dissociating into ($NH_2$ + $H_2$), the bond lengths [$R_{(NH)TS}$] at the transition state is ≅1.590 Å. The energy barrier heights of $^2A_1$ from the transition state to $NH_4$ and [$NH_2^*(A^2A_1)$ + $H_2$] are ≅3.59 and 1.06 eV, respectively. The heights of $^2B_1$ from the transition state to $NH_4$ and [$NH_2(X^2B_1)$ + $H_2$] are ≅2.96 and 4.66 eV, respectively. The energy gaps of $^2A_1$ and $^2B_1$ between $NH_4$ and ($NH_2$ + $H_2$) are -2.53 and -1.69 eV, respectively. Although the ground state of the $NH_4$ radical has an energy barrier of ≅0.83 eV along the NH bond rupture, the stability of $NH_4$ is found to be influenced by tunneling. The bond breaking takes place near the equilibrium geometry of $NH_4$. But, the existence of $NH_4$ has been confirmed by the various methods.[20-32] The lifetime of $NH_4$ was measured experimentally to be 13 ps, a value more than $10^6$ times shorter than in the one for $NH_4$ in ammonia clusters.[1-19]

Smith *et al.*,[23,27] Kassab *et al.*,[21,22] and Cardy *et al.*[25] have calculated the ground potential energy curve of the $NH_4$ radical dissociating into ($NH_3$ + H) and ($NH_2$ + $H_2$). Its bond distances at the equilibrium [$R_{(NH)eq}$] obtained by CIPSI (equivalent to a multireference Möller-Plesset second order method) and SDCI are ≅1.04 and 1.03 Å, respectively. And the bond distances [$R_{(NH)TS}$] at the transition state are ≅1.37 and 1.43 Å, respectively. The barrier heights from the transition state to $NH_4$ are ≅0.88 and 0.85 eV, respectively. The potential curves for the dissociation of $NH_4$ into its products are endothermic by -0.23 and -0.21 eV, respectively. And the energy gap between ($NH_3$ + H) and ($NH_2$ + $H_2$) is 0.1 eV.

As shown in Table I, our result for the formation reaction of $NH_4$ from ($NH_2$ + $H_2$) is slightly endothermic by -0.22. By the weak interaction between the nuclear and a Rydberg electron, the ionization and excitation energies of $NH_4$ are relatively low, that is, the excitation energies of the Rydberg transitions (3s→higher orbitals) should be lower than $E_{(I.P.)}$≅4.57 eV. Our results are similar to the other theoretical results,[22,23] but different from those characterized by Herzberg,[5] that is, the excitation energies of (3s→3d) and (3p→3d) observed by the experiment are 2.19 and 1.87 eV, respectively. Meanwhile, the geometric structure of $NH_4$ is similar to that of $NH_4^+$ and the Rydberg $NH_4$ radical is a semi-ionic structure described as $(NH_4^+)(e^-)_{3s}$. The geometric structure of $NH_4^+$ with the $T_d$ symmetry is more stable than that of $NH_3$ with $C_{3v}$. Therefore, the proton affinity of $NH_3$ is relatively large. Since the ionization from $NH_3$ to $NH_3^+$ comes to change the geometric structure from the $C_{3v}$ symmetry to $D_{3h}$, the ionization and excitation energies of $NH_2$ and $NH_3$ are relatively large. Our results are in good agreement with the experimental[4,5,11,70,75] and theoretical[22,23,27,30,71-74,76-81] results.

Under the $C_{2v}$- and $C_s$-symmetry constraints, the potential energy curves for the $^2A_1$ and $^2B_1$ states of the Rydberg $NH_4$ radical dissociating into ($NH_3$ + H) and ($NH_2$ + $H_2$) are drawn in Figure 1. The potential energy curve for the ground state of $NH_4$ dissociating into ($NH_3$ + H) is progressed with $C_{2v}$-symmetry. From equilibrium to $R_{(NH)}$≅2.0 Å, the dissociation reaction of $NH_4$ into ($NH_2$ + $H_2$) is progressed with $C_{2v}$-symmetry. The potential energy curve of the ground state ($^2A_1$) of $NH_4$ correlates to the [$NH_2^*(A^2A_1$ + $H_2(X^1\Sigma_g^+)$] asymptote. From $R_{(NH)}$≅2.0 Å to their dissociation products, the reaction is progressed with $C_s$-symmetry. The potential curve correlates to the product limits of [$NH_2(X^2B_1)$ + $H_2(X^1\Sigma_g^+)$]. As the results, the symmetry breaking in the corrrelation diagram is occurred at $R_{(NH)}$≅2.0 Å. Cardy *et al.*[25] have analyzed the correlation curves for the dissociation of $NH_4$ into ($NH_2$ + $H_2$) under the $C_{2v}$- and $C_s$-symmetry constraints. Their potential curves emerging from the [$NH_2^*(A^2A_1)$ + $H_2(X^1\Sigma_g^+)$] and [$NH_2(X^2B_1)$ + $H_2(X^1\Sigma_g^+)$] asymptotes are crossed behind the rate determining step of the insertion of $H_2$ into $NH_2$. The rate determining step of the reaction is not a transition state but a critical point. They have concluded that the insertion process occurs via a two-step mechanism along the crossing of the $C_s$ saddle point.

The potential energy curves for the ground and low lying excited states of the Rydberg $NH_4$ radical dissociating into ($NH_3$ + H) are drawn in Figure 2. The potential energy of the $NH_4$ radical is set equal to zero. Because of the complexity of the excited states, we have cut the potential energy curves of the high lying excited states at $R_{(NH)}$=1.2 Å and have not connected the curves between $R_{(NH)}$=4.0 Å and the ($NH_3$ + H) asymptote. We have drawn a few low lying states and they are labeled as $1^2A_1$, $2^2A_1$, $3^2A_1$, $4^2A_1$, and $1^2E$. The ground $^2A_1$ state of the $NH_4$ radical correlates with an antibonding interaction of the [$NH_3(^1A_1)$ + $H(^2S)$] asymptote. This curve is quasibound, which means that its equilibrium energy is higher than that of the dissociation asymptote of ($NH_3$ + H). The potential curve has a potential barrier near the equilibrium geometry of $NH_4$. It is made by an avoided curve crossing between the dissociative diabatic state of the Rydberg [$(NH_4^+)(e^-)_{3s}$] radical and the repulsive diabatic state emerging from an antibonding interaction of the [$NH_3(^1A_1)$ + $H(^2S)$]

asymptote. The barrier height and potential well are very low and shallow, respectively. The maximum position [$R_{(NH)}$≅1.40 Å] of the transition state of the ground potential curve is located out of line of those [$R_{(NH)}$≅1.95 Å] of the first and second excited states with the $^2A_1$ symmetry.

In Figure 2, all potential curves of the excited states are shallowly bound. While, the third excited $^2A_1$ state is bound at relatively wide range (between $R_{(NH)}$≅2.0 and 6.0 Å). All potential barriers of the excited states are formed by the curve crossings. The first curve crossings between the dissociative diabatic excited states of [$(NH_4^+)(e^-)_{Rydberg}$] and the repulsive diabatic states from the antibonding interaction of [$NH_3(^1A_1)$ + $H(^2S)$] are found between $R_{(NH)}$≅1.6 and 2.0 Å. The second curve crossings between the dissociative diabatic excited states of [$(NH_4^+)(e^-)_{Rydberg}$] and the repulsive diabatic states from the antibonding interaction of [$NH_3(^3A_1$; n→3s) + $H(^2S)$] are also found from $R_{(NH)}$≅2.0 to 2.25 Å. The first excited $^2E$ state emerging from $NH_4$ (3s→$3p_{x,y}$) directly correlates with an attractive state from the [$NH_3^+(e^-)_{3px,y}$ + H] asymptote. The second excited $^2E$ state is bound at wide range [between $R_{(NH)}$≅2.5 and 6.0 Å]. The wide potential well is made from curve crossing between the dissociative diabatic excited state of [$(NH_4^+)(e^-)_{Rydberg}$] and the repulsive diabatic state emerging from an antibonding interaction of [$NH_3(^3E)$ + $H(^2S)$]. The potential barrier by the avoided curve crossing exists at $R_{(NH)}$≅2.2 Å.

Adiabatic and diabatic potential energy curves of the dissociation of $NH_4$ into ($NH_3$ + H) have been constructed by Kassab and Evleth[21,22] According to their curves, the ground $^2A_1$ state surface along the NH bond rupture has a potential energy barrier which is made from the avoided curve crossing. In the diabatic potential curves, the diabatic curve crossings between the repulsive state emerging from ($NH_3$ + H) and the dissociative states of the ground and excited $^2A_1$ states of $NH_4$ have been drawn by the broken lines. But, in the adiabatic curves, the potential wells and barriers formed by the avoided crossings have not been represented clearly. And the maximum positions of the potential barriers for the ground and excited potential curves are drawn to be out of line of the repulsive diabatic curve emerging from the ($NH_3$ + H) asymptote. Particularly, in their Figure 2, the adiabatic and diabatic potential correlation curves with the $^2A_1$ symmetry are quite different from each other.

To investigate the avoided curve crossing clearly, the potential energy curves for the ground and low lying excited $^2A_1$ states are presented in Figure 3. The broken lines indicate estimated diabaticc potential energy curves and these are drawn by hands. The ground $^2A_1$ state interconnects the $NH_4$ structure with the ($NH_3$ + H) asymptote. In the $NH_4$ radical dissociating into ($NH_3$ + H), the ground Rydberg $NH_4$ radical diabatically dissociates into two kinds of the asymptotes, that is, $NH_4$ diabatically dissociates into the first excited [$(H_3N^+)(e^-)_{3s}$ + $H(^2S)$] and the ion-ion pair [$H_3N^+(^2A_2'')$ + $H^-(^1S)$] asymptotes. In the second dissociation, the pair has strongly attractive ion character as an ion approaches to the other. The diabatic potential well should be very deep. As the result, the avoided curve crossings take place around $R_{(NH)}$≅1.5 Å. The barrier height of the ground correlation curve is found to be low.

As shown in Figure 3, the $2^2A_1$ state is shallowly bound. The barrier around $R_{(NH)}$≅2.0 Å is formed from the curve crossing between the attractive state from [$NH_3^+$ + $H^-$] and the repulsive state from [$NH_3$ + H]. The $3^2A_1$ state emerging from the [$(NH_3^+)(e^-)_{3s}$ + $H(^2S)$] asymptote is diabatically repulsive. By the avoided curve crossings, this state is very shallowly bound around $R_{(NH)}$≅2.0 Å. The $4^2A_1$ state is widely bound due to two avoided curve crossings between $R_{(NH)}$≅2.0 and 6.0 Å. Meanwhile, when the internuclear distance between $NH_3^+$ and $H^-$ become short, the attractive state emerging from an ion-ion pair [$NH_3^+$ + $H^-$] diabatically correlates with $NH_4$. This state is diabatically bound due to the strongly ion-ion electrostatic attraction. Therefore, around three positions ($R_{(NH)}$≅2.0, 6.0, and 12.0 Å), the curve crosses with the diabatic potential curves of the $^2A_1$ states emerging from the different asymptotes.

The potential energy curves for the several low lying $^2A_1$ states of the Rydberg $NH_4$ radical dissociating into ($NH_2$ + $H_2$) are drawn in Figure 4. And they are labeled as $1^2A_1$, $2^2A_1$, $3^2A_1$, and $1^2B_1$. The ground $^2A_1$ state of the $NH_4$ radical correlates to the [$NH_2^*(1^2A_1)$ + $H_2(X^1\Sigma_g^+)$] asymptote. The potential curve has a potential barrier near the equilibrium geometry of $NH_4$. It is made by an avoided curve crossing between the dissociative diabatic state of the Rydberg [$(NH_4^+)(e^-)_{3s}$] radical and the repulsive diabatic state emerging from an antibonding interaction of the [$NH_2^*(1^2A_1)$ + $H_2(X^1\Sigma_g^+)$] asymptote. The barrier height and potential well are slightly high and shallowly bound, respectively. The energy gap between [$NH_2(1^2B_1)$ + $H_2(X^1\Sigma_g^+)$] and [$NH_2^*(1^2A_1)$ + $H_2(X^1\Sigma_g^+)$] is 2.21 eV.

All potential energy curves emerging from the antibonding interactions of the [$NH_2^*(^2A_1)$ + $H_2(X^1\Sigma_g^+)$] asymptotes are diabatically repulsive, while a potential energy curve emerging from the [$NH_2^+(A^1A_1)$ + $H_2^-(X^2\Sigma_u^+)$] asymptote is diabatically attractive. As a results, at shorter than $R_{(NH)}$≅2.0 Å, the avoided curve crossings between the dissociative diabatic states of [$(NH_4^+)(e^-)_{Rydberg}$] and the repulsive diabatic states from [$NH_2$ + $H_2(X^1\Sigma_g^+)$] are occurred. At larger than $R_{(NH)}$≅2.0 Å, the curve crossings between the diabatically attractive diabatic state emerging from [$NH_2^+(A^1A_1)$ + $H_2^-(X^2\Sigma_u^+)$] and the diabatically repulsive diabatic states from [$NH_2$ + $H_2(X^1\Sigma_g^+)$] are found. Therefore, all potential barriers of the $^2A_1$ states are formed by the curve crossings.

Adiabatic potential energy curves for the dissociation of $NH_4$ into ($NH_2$ + $H_2$) have been constructed by Kassab and Evleth[21,22] and Cardy *et al.*[25] In the potential energy curve of Kassab and Evleth, the three states emerging from the dissociative states of $NH_4$ directly correlates to the three repulsive states from the ($NH_2$ + $H_2$) asymptote under the $C_{2v}$-symmetry constraints. By the avoided curve crossings between the dissociative states and the repulsive states, the barriers are formed at shorter than $R_{(NH)}$≅2.0 Å. When $H_2$ molecule approaches the three valence states of $NH_2$, these states are repulsive. Particularly, Cardy *et al.* has analyzed the detailed geometric representation of the insertion mechanism, the quantitative state correlation diagram, and the relaxation of a $C_{2v}$ reaction path between $NH_4$ and ($NH_2$ + $H_2$). The quantitative state correlation diagram and relaxation of a $C_{2v}$ reaction path have been represented in detail. But the adiabatic potential curves and barriers formed by the avoided crossings have not been represented clearly.

Now the question is why the maximum positions of the ground and excited states are found to be out of line of the repulsive diabatic curve emerging from the antibonding interaction of [$NH_3(^1A_1)$ + $H(^2S)$] and [$NH_2$ + $H_2(X^1\Sigma_g^+)$]. To analyze the curve crossing, we have investigated the contributions of the dominant configuration to the total wave functions of the $^2A_1$ states and listed them in Table II and III. For $NH_4$ dissociating into ($NH_3$ + H) and ($NH_2$ + $H_2$), the dominant configuration for the ground $^2A_1$ state is [core]$2a_1^2\ 1t_1^6\ 3a_1^1$ at the $NH_4$ structure, [core]$2a_1^2\ 1e_1^4\ 3a_1^2\ (4a_1^1)_H$ at the ($NH_3$ + H) asymptote, and [core]$2a_1^2\ 1b_2^2\ 3a_1^1\ 1b_1^2\ (5a_1^2)_{H2}$ at the ($NH_2$ + $H_2$) asymptote. $2a_1^2\ 1t_1^6$ is an electronic configuration of $NH_4^+$. $3a_1^1$ indicates an electron of the Rydberg 3s orbital having a $NH_4^+$ structure as a core. Therefore, the electronic structure of $NH_4$ indicates as $NH_4^+(e^-)_{3s}$. Along N-H bond rupture, a $1t_1$ orbital of $NH_4$ separates into two orbitals ($1e_1$ and $3a_1$) in $NH_3$. The $4a_1$ orbital is nonbonding, i.e., a character of 1s of H. $4a_1^1$ indicates one electron in the 1s orbital of H. As the result, the configuration of $2a_1^2\ 1e_1^4\ 3a_1^2\ (4a_1^1)_H$ at $R_{(NH)}$=14.0 Å indicates the antibonding pair [$NH_3(^1A_1)$ + $H(^2S)$] asymptote. For $NH_2$-$H_2$ bond rupture, a $1t_1$ orbital of $NH_4$ separates into two orbitals ($1b_2$ and $3a_1$) in $NH_2$. The $5a_1$ orbital is a character of $1\sigma$ of $H_2$. $5a_1^2$ indicates two electrons in the $1\sigma$ orbital of $H_2$. Therefore, the configuration of $2a_1^2\ 1b_2^2\ 3a_1^1\ 1b_1^2\ (5a_1^2)_{H2}$ at $R_{(NH)}$=8.0 Å indicates the antibonding pair [$NH_2^*(1^2A_1)$ + $H_2(X^1\Sigma_g^+)$] asymptote.

As shown in Table II, the dominant configurations of the [$H_3N(^3A_1;n\rightarrow 3s)$ + $H(^2S)$] and [$NH_3^+(^2A_2'')$ + $H^-(^1S)$] asymptotes are $\underline{222111}$ and $\underline{22212}$, respectively. In the diabatic dissociation of $NH_4$ into [$(H_3N^+)(e^-)_{3s}$ + $H(^2S)$], the contribution for the configration of $\underline{222111}$ begins to appear the first excited $^2A_1$ state at $R_{(NH)}$=1.5 Å and the contribution of it increases with internuclear distance. From $R_{(NH)}$=5.0 Å, it become a dominant configuration in the first $^2A_1$ state. In the diabatic dissociation of $NH_4$ into the ion-ion pair $[H_3N^+(^2A_2'') + H^-(^1S)]$ asymptote, the contribution for the configration of 22212 represents the first excited $^2A_1$ state from $R_{(NH)}=1.5$ to 4.0 Å. At $R_{(NH)}=5.0$ Å, the contribution represents the second excited state. Between $R_{(NH)}=6.0$ and 10.0 Å, it represents the third excited state. This configuration can have an attractive ion character as an ion approaches another. These two attractive diabatic curves cross with the repulsive diabatic curve emerging from an antibonding interaction of the $[NH_3(^1A_1) + H(^2S)]$ asymptote. Two attractive diabatic characters greatly influence the curve crossing, that is, the contributions of those chatacters are larger than that of the repulsive chatacter. As the result, the potential energy barrier of the ground $^2A_1$ state is shifted to the equilibrium geometry of $NH_4$. And the barrier height appears to be low. Particularly, the avoided curve crossing between repulsive curve emerging from an antibonding interaction of the $[NH_3(^1A_1) + H(^2S)]$ and the strongly attractive curve from $[H_3N^+(^2A_2'') + H^-(^1S)]$ greatly influences the potential barrier of the ground correlation curve.

In the excited $2^2A_1$ state, the dominant configuration is $2a_1^2\ 1t_1^6\ (3p_z)^1_{\text{Rydberg}}$ at shorter than $R_{(NH)}\cong 1.1$ Å, $2a_1^2\ 1e_1^4\ 3a_1^2\ (3p_z)^1_{\text{Rydberg}}$ between $R_{(NH)}\cong 1.1$ and 2.1 Å, $(2a_1')^2\ (1e_1')^4\ (1a_2'')^1\ (1s)^2_H$ between $R_{(NH)}\cong 2.2$ and 4.0 Å, and $(2a_1')^2\ (1e_1')^4\ (1a_2'')^1\ (3s)^1_{\text{Rydberg}}\ (1s)^1_H$ at larger than $R_{(NH)}\cong 5.0$ Å. In the dissociation of $NH_4$ into $(NH_3 + H)$, $2a_1^2\ 1t_1^6\ (3p_z)^1_{\text{Rydberg}}$ at shorter than $R_{(NH)}\cong 1.1$ Å represents the $(NH_4^+)(e^-)_{3pz}$ structure, $2a_1^2\ 1e_1^4\ 3a_1^2\ (3p_z)^1_{\text{Rydberg}}$ between $R_{(NH)}\cong 1.1$ and 2.1 Å represents $(NH_3 \ldots H^+)(e^-)_{3pz}$, $(2a_1')^2\ (1e_1')^4\ (1a_2'')^1\ (1s)^2_H$ between $R_{(NH)}\cong 2.2$ and 4.0 Å represents $(NH_3^+ \ldots H^-)$, and $(2a_1')^2\ (1e_1')^4\ (1a_2'')^1\ (3s)^1_{\text{Rydberg}}\ (1s)^1_H$ at larger than $R_{(NH)}\cong 5.0$ Å represents $[(H_3N^+)(e^-)_{3s} + H]$. More interestingly, the $2^2A_1$ state between $R_{(NH)}\cong 2.2$ and 4.0 Å has a dominant configuration of $(2a_1')^2\ (1e_1')^4\ (1a_2'')^1\ (1s)^2_H$ which means an ion-ion interaction structure as $(NH_3^+ \ldots H^-)$. Here one electron jumped from the Rydberg $3p_z$ orbital of $NH_3$ to the 1s orbital of H. Therefore, this state has strongly attractive ion character.

The dominant configuration of the $3^2A_1$ state is $2a_1^2\ 1t_1^6\ (4s)^1_{\text{Rydberg}}$ at shorter than $R_{(NH)}\cong 2.0$ Å, $(2a_1')^2\ (1e_1')^4\ (1a_2'')^1\ (1s)^2_H$ between $R_{(NH)}\cong 2.0$ and 2.1 Å, $2a_1^2\ 1e_1^4\ 3a_1^2\ (3p_z)^1_{\text{Rydberg}}$ between $R_{(NH)}\cong 2.2$ and 3.5 Å, $(2a_1')^2\ (1e_1')^4\ (1a_2'')^1\ (1s)^2_H$ between $R_{(NH)}\cong 4.0$ and 5.0 Å, and $(2a_1')^2\ (1e_1')^4\ (1a_2'')^1\ (3s)^1_{\text{Rydberg}}\ (1s)^1_H$ at larger than $R_{(NH)}\cong 5.0$ Å. In the electronic structure, $2a_1^2\ 1t_1^6\ (4s)^1_{\text{Rydberg}}$ represents $(NH_4^+)(e^-)_{4s}$, $(2a_1')^2\ (1e_1')^4\ (1a_2'')^1\ (1s)^2_H$ represents $(NH_3^+ \ldots H^-)$, $2a_1^2\ 1e_1^4\ 3a_1^2\ (3p_z)^1_{\text{Rydberg}}$ represents $[(NH_3)\ldots(H^+)](e^-)_{3pz}$, and $(2a_1')^2\ (1e_1')^4\ (1a_2'')^1\ (3s)^1_{\text{Rydberg}}\ (1s)^1_H$ represents $[(NH_3^+)(e^-)_{3s} + H]$. Around $R_{(NH)}\cong 2.05$ and 4.5 Å, the dominant configuration represents $(2a_1')^2\ (1e_1')^4\ (1a_2'')^1\ (1s)^2_H$ which means the attractive interaction of $[NH_3^+ \ldots H^-]$. In the $4^2A_1$ state, the dominant configuration between $R_{(NH)}\cong 2.3$ and 5.0 Å is $(2a_1')^2\ (1e_1')^4\ (1a_2'')^1\ (3s)^1_{\text{Rydberg}}\ (1s)^1_H$ of a repulsive character emerging from the $[(NH_3^+)(e^-)_{3s} + H]$ asymptote. The dominant configuration between $R_{(NH)}\cong 6.0$ and 10.0 Å is $(2a_1')^2\ (1e_1')^4\ (1a_2'')^1\ (1s)^2_H$ having the $(NH_3^+ + H^-)$ character. The changes of these configurations are in accordance with the potential energy curves in Figure 3.

As shown in Table III, the dominant configurations of the $[H_2N(2^2A_1;n\rightarrow 3s) + H_2(X^1\Sigma_g^+)]$ and $[NH_2^+(A^1A_1) + H_2^-(X^2\Sigma_u^+)]$ asymptotes are 222012 as a $[\text{core}]2a_1^2\ 1b_2^2\ 3a_1^2\ 1b_1^0\ 4a_1^1\ (5a_1^2)_{H2}$ configuration and 222021 as a $[\text{core}]2a_1^2\ 1b_2^2\ 3a_1^2\ 1b_1^0\ (5a_1^2\ 6a_1^1)_{H2}$, respectively. In the diabatic dissociation of $NH_4$ into $[(H_2N)(e^-)_{3s} + H_2(X^1\Sigma_g^+)]$, the contribution for the configuration of 222012 begins to appear in $2^2A_1$ at $R_{(NH)}=1.5$ Å and the contribution of it increases with internuclear distance. From $R_{(NH)}=2.1$ Å, it become a dominant configuration in $2^2A_1$. In the diabatic dissociation of $NH_4$ into the ion-ion pair $[NH_2^+(A^1A_1) + H_2^-(X^2\Sigma_u^+)]$ asymptote, the contribution for the configuration of 222021 is represented in the $2^2A_1$ state from $R_{(NH)}=1.5$ to 2.0 Å. Although the configurations from $4^2A_1$ to $7^2A_1$ have not listed in Table III, the contribution will be represented between $R_{(NH)}=2.2$ and 8.0 Å. The attractive diabatic character greatly influences the curve crossing. As a result, the potential energy barriers of the $1^2A_1$ and $2^2A_1$ states are shifted to the equilibrium geometry of $NH_4$.

In the excited $2^2A_1$ state, the dominant configuration is $2a_1^2\ 1t_1^6\ (3p_z^1)_{Rydberg}$ at shorter than $R_{(NH)}\cong1.1$ Å, $2a_1^2\ 1b_2^2\ 3a_1^1\ 1b_1^2\ (5a_1^2)_{Rydberg}$ between $R_{(NH)}\cong1.2$ and 1.4 Å, $2a_1^2\ 1b_2^2\ 3a_1^2\ 1b_1^0\ (5a_1^2\ 6a_1^1)_{H2}$ between $R_{(NH)}\cong1.5$ and 2.0 Å, and $2a_1^2\ 1b_2^2\ 3a_1^2\ 1b_1^0\ (4a_1^1)_{Rydberg}\ (5a_1^2)_{H2}$ at larger than $R_{(NH)}\cong2.1$ Å. In the electron structure, $2a_1^2\ 1t_1^6\ (3p_z^1)_{Rydberg}$ at shorter than $R_{(NH)}\cong1.1$ Å represents the $(NH_4^+)(e^-)_{3pz}$ structure, $2a_1^2\ 1b_2^2\ 3a_1^1\ 1b_1^2\ (5a_1^2)_{Rydberg}$ between $R_{(NH)}\cong1.2$ and 1.4 Å represents $(NH_2\ldots H_2)^+(e^-)_{3pz}$, $2a_1^2\ 1b_2^2\ 3a_1^2\ 1b_1^0\ (5a_1^2\ 6a_1^1)_{H2}$ between $R_{(NH)}\cong1.5$ and 2.0 Å represents $(NH_2^+\ldots H_2^-)$, and $2a_1^2\ 1b_2^2\ 3a_1^2\ 1b_1^0\ (4a_1^1)_{Rydberg}\ (5a_1^2)_{H2}$ at larger than $R_{(NH)}\cong2.1$ Å represents $[(H_2N^+)(e^-)_{3s} + H_2]$. Particularly, the dominant configuration of $2^2A_1$ between $R_{(NH)}\cong1.5$ and 2.0 Å means an ion-ion interaction structure $(NH_2^+\ldots H_2^-)$ as $2a_1^2\ 1b_2^2\ 3a_1^2\ [(1\sigma)^2\ (1\sigma^*)^1]_{H2}$.

The dominant configuration of the $3^2A_1$ state is $2a_1^2\ 1t_1^6\ (4s^1)_{Rydberg}$ at shorter than $R_{(NH)}\cong1.1$ Å, $2a_1^2\ 1b_2^2\ 3a_1^1\ 1b_1^2\ (5a_1^2)_{Rydberg}$ between $R_{(NH)}\cong1.2$ and 1.4 Å, $2a_1^2\ 1b_2^2\ 3a_1^2\ 1b_1^0\ (4a_1^1)_{Rydberg}\ (5a_1^2)_{H2}$ between $R_{(NH)}\cong1.5$ and 1.6 Å, $2a_1^2\ 1b_2^2\ 3a_1^2\ 1b_1^0\ (5a_1^2\ 6a_1^1)_{H2}$ between $R_{(NH)}\cong1.8$ and 2.3 Å, and $2a_1^2\ 1b_2^2\ 3a_1^2\ 1b_1^0\ (3p_x^1)_{Rydberg}\ (5a_1^2)_{H2}$ at larger than $R_{(NH)}\cong2.3$ Å. In the electronic structure, $2a_1^2\ 1t_1^6\ (4s^1)_{Rydberg}$ represents $(NH_4^+)(e^-)_{4s}$, $2a_1^2\ 1b_2^2\ 3a_1^1\ 1b_1^2\ (5a_1^2)_{Rydberg}$ represents $[(NH_2^*)\ldots(H_2)]$, $2a_1^2\ 1b_2^2\ 3a_1^2\ 1b_1^0\ (4a_1^1)_{Rydberg}\ (5a_1^2)_{H2}$ represents $[(NH_2)\ldots(H_2^+)](e^-)_{3s}$, $2a_1^2\ 1b_2^2\ 3a_1^2\ 1b_1^0\ (5a_1^2\ 6a_1^1)_{H2}$ represents $(NH_2^+\ldots H_2^-)$, and $2a_1^2\ 1b_2^2\ 3a_1^2\ 1b_1^0\ (3p_x^1)_{Rydberg}\ (5a_1^2)_{H2}$ represents $[(NH_2^+)(e^-)_{3px} + H_2]$. Between $R_{(NH)}\cong1.8$ and 2.3 Å, the dominant configuration represents $2a_1^2\ 1b_2^2\ 3a_1^2\ [(1\sigma)^2\ (1\sigma^*)^1]_{H2}$ which means the attractive interaction of $[NH_2^+\ldots H_2^-]$. When the internuclear distance between $NH_2^+$ and $H_2^-$ become short, the attractive state emerging from an ion-ion pair $[NH_2^+ + H_2^-]$ diabatically correlates to $NH_4$. This state is diabatically bound due to the ion-ion electrostatic attraction. These dominant configurations are in accordance with the avoided curve crossings of Figure 4.

## 3.2 Potential Curves of $H_3O$ Dissociating into its Asymptote

Geometric parameters at the equilibrium and transition states, the relative energies of $H_3O$ dissociating into ($H_2O$ + H) and (OH + $H_2$), and the ionization and excitation energies of $H_3O$, $H_2O$, OH, and $H_2$ are listed in Table IV. Our results for $H_3O$ calculated by the SDCI, MP2, and CCSD(t) methods are in line with the experimental[10,37,40,49,84,85,93-95] and theoretical[43,44,46,47,87-92] values. Since the ground state of $H_3O$ has an electron in a Rydberg 3s orbital, $H_3O$ is a semi-ionic structure described as $(H_3O^+)(e^-)_{3s}$. At the equilibrium internuclear distance, $R_{(OH)eq}$ calculated with the SDCI and CCSD(t) methods are ≅1.022 and 1.020 Å, respectively. $R_{(OH)eq}$ of $H_3O$ is longer than that [$R_{(OH)eq}\cong0.962$ Å) of $H_2O$.

For the $^2A_1$ state of $H_3O$ dissociating into ($H_2O$ + H) and (OH + $H_2$), $R_{(OH)TS}$ at the SDCI level are ≅1.213 and ≅1.513 Å. The relative energy differences from the transition state to $H_3O$ and ($H_2O$ + H) are ≅0.12 and ≅0.97 eV, respectively. The energy differences from the transition state to $H_3O$ and $[OH(A^2\Sigma^+) + H_2]$ are ≅4.99 and ≅1.14 eV, respectively. The energy gaps between $H_3O$ and ($H_2O$ + H) and between $H_3O$ and $[OH(A^2\Sigma^+) + H_2(X^1\Sigma_g^+)]$ are -0.86 and -3.85 eV, respectively. In the $^2B_1$ state of $H_3O$ dissociating into (OH + $H_2$), $R_{(OH)eq}$ and $R_{(OH)TS}$ are ≅1.019 and ≅1.501 Å, respectively. The energy differences from the transition state to $H_3O$ and $[OH(X^2\Pi) + H_2(X^1\Sigma_g^+)]$ are ≅5.02 and 7.18 eV, respectively. The energy gap of $^2B_1$ between $H_3O$ and $[OH(X^2\Pi) + H_2(X^1\Sigma_g^+)]$ is -2.15 eV. Because the ground potential curve has a very low barrier, $H_3O$ is very unstable. That is, the bond breaking takes place near the equilibrium geometry of $H_3O$. As a result, the existence of $H_3O$ has not been observed experimentally.

The ground potential energy curve of the $H_3O$ radical dissociating into ($H_2O$ + H) were calculated by Niblaeus *et al.*[46] and Luo and Jungen[49]. At the equilibrium geometry, the bond distances [$R_{(OH)eq}$] are ≅1.053 and ≅1.02 Å, respectively. The bond angles (∠HOH) are ≅101.8 and ≅106.9 degree, respectively. And the bond distance [$R_{(OH)TS}$] at the transition state is ≅1.248 Å. The barrier heights from the transition state to $H_3O$ are ≅0.13 and ≅0.08 eV, respectively. The energy gaps between $H_3O$ and ($H_2O$ + H) calculated by CI and CEPA methods are -0.89 and -1.0 eV, respectively. Meanwhile, in investigations performed by Melton and Joy,[37] the structure of $H_3O$ has a planar geometry. The bond distance [$R_{(OH)eq}$] is ≅1.053 Å. They predicted that the $H_3O$ radical is stable relative to ($H_2O$ + H).

As shown in Table IV, our results for the formation of $H_3O$ from its asymptotic products are slightly endothermic by 0.12 eV. By the weak interaction between the nuclear and a Rydberg electron, the geometric structure of $H_3O$ is similar to that of $H_3O^+$. The ionization and excitation energies of $H_3O$ are relatively low. That is, the excitation energies of the Rydberg transitions (3s→higher orbitals) should be lower than the ionization potential of ≅5.30 eV. On the other hand, the ionization potential and proton affinity of $H_2O$ are ≅12.54 and ≅7.32 eV at the SDCI level, respectively. The ionization energy (≅12.71 eV) and electron affinity (≅1.81 eV) of OH are relatively large. The ionization potential and electron affinity of $H_2$ are ≅15.43 and ≅1.38 eV, respectively. The potential energy curves for the $^2A_1$ and $^2B_1$ states of the Rydberg $H_3O$ radical dissociating into its dissociation product are drawn in Figure 5. The potential energy curves for the dissociation reactions of ($H_2O$ + H) and (OH + $H_2$) are slightly endothermic. The energy gap between [$OH(X^2\Pi_1) + H_2(X^1\Sigma_g^+)$] and [$H_2O(X^1A_1) + H(^2S)$] asymptotes is ≅0.66 eV. The energy gap between [$OH(X^2B_1) + H_2(X^1\Sigma_g^+)$] and [$OH(A^2\Sigma^+) + H_2(X^1\Sigma_g^+)$] asymptotes is ≅4.0 eV.

The thermodynamic cycle based on the experimental results was drawn by Williams and Porter.[10] The energies of $H_3O$ dissociating into ($H_2O$ + H) in the Na and K target atoms are -1.12±0.07 and -1.57±0.07 eV, respectively. The fragmentation energies of the $H_3O$ radical dissociating into (OH + $H_2$) in the Na and K target atoms are -0.54±0.03 and -0.74±0.04 eV, respectively. The vertical electron affinities of $H_3O^+$ in the Na and K targets are 5.3 and 5.0 eV, respectively. The relative energy level of the ($H_2O$ + H) asymptote is 15 kcal/mol stable with respect to that of the (OH + $H_2$) asymptote. A metastable state of $H_3O$ with a lifetime greater than $10^{-7}$ sec was not obtained. ESR spectrum of matrix-stabilized hydronium $H_3O$ is obtained by Martin and Swift.[38] $H_3O$ is stable by bond dissociation energy of 7 kcal/mol relative to ($H_2O$ +H). In the experiments performed by Gellene and Porter,[40] the $H_3O$ radical is obtained from an electron capture process of their parent ion in a collision with a beam of metal atoms. The apparent electron affinity determined by fragmentation energy is 3.88 eV. The ionization potential and transition energy (3s→3p) of $D_3O$ are estimated to be 4.3±0.1 and 1.6 eV, respectively. Raynor *et al.*[47] have calculated transition energy (3s→3p) to be the range of 1.87 - 2.25 eV for $H_3O$ and the ionization potential of 4.68 eV.

Under the $C_{2v}$ symmetry constraints, the potential energy curves for the ground and low lying excited states of $H_3O$ dissociating into ($H_2O$ + H) and (OH + $H_2$) are drawn in Figure 6 and 7, respectively. And they are labeled as $1^2A_1$, $2^2A_1$, $3^2A_1$, $4^2A_1$, $1^2B_1$, and $2^2B_1$, respectively. The ground $^2A_1$ state of $H_3O$ correlates with a repulsive state emerging from an antibonding interaction of the [$H_2O(^1A_1) + H(^2S)$] and [$OH(A^2\Sigma^+) + H_2(X^1\Sigma_g^+)$] asymptote. It is made by an avoided curve crossing between the dissociative diabatic state of the Rydberg [$(H_3O^+)(e^-)_{3s}$] radical and the repulsive diabatic state emerging from the [$H_2O(^1A_1) + H(^2S)$] and [$OH(A^2\Sigma^+) + H_2(X^1\Sigma_g^+)$] asymptotes. This curve is quasibound, which means that its equilibrium energy is higher than that of the dissociation asymptote of its dissociation products. The barrier height and potential well are very low and shallow, respectively. The potential curve has an energy barrier near the equilibrium geometry of $H_3O$. In the ground potential energy curve, the maximum position [$R_{(OH)}$≅1.213 Å] of the transition state is located out of line of those of the first and higher excited states.

In $H_3O$ dissociating into ($H_2O$ + H) of the Figure 6, the ground Rydberg $H_3O$ radical diabatically dissociates into the first excited [$H_2O(^1A_1; 1b_1 \rightarrow 3p_{x,y}) + H(^2S)$] and the ion-ion pair [$H_2O^+(^2A_1) + H^-(^1S)$] asymptotes. In the second dissociation path, one electron jumps from the $1b_1$ orbital of $H_2O$

to the 1s orbital of H. The ion pair has strongly attractive ionic character as an ion approaches to the other. By the avoided curve crossing between strongly attractive ionic states emerging from [$H_2O^+(^2A_1)$ + $H^-(^1S)$] and the repulsive diabatic state from [$H_2O(^1A_1)$ + $H(^2S)$], the potential energy barrier of the ground $^2A_1$ state is shifted to the equilibrium geometry of $H_3O$. The barrier height is found to be low. All potential curves of the excited states formed by the curve crossings are bound between $R_{(OH)}$≅2.0 Å and ≅4.0 Å. In the first $2^2A_1$ state, the curve crossings between the dissociative diabatic excited states of [$(H_3O^+)(e^-)_{Rydberg}$] and the repulsive diabatic states from the antibonding interaction of [$H_2O(^1A_1;\ 1b_1 \rightarrow 3p_{x,y})$ + $H(^2S)$] are found between $R_{(OH)}$≅1.5 Å and ≅4.0 Å. Because of the energy barrier formed by the curve crossing, the potential curve is bound around $R_{(OH)}$≅2.5 Å. The $3^2A_1$ state emerging from the [$H_2O(^1A_1;\ 1b_1 \rightarrow 3p_{x,y})$ + $H(^2S)$] asymptote is diabatically repulsive. By the avoided curve crossings, this state is shallowly bound around $R_{(OH)}$ ≅3.75 Å. The first excited $^2E$ state emerging from $H_3O$ ($3s \rightarrow 3p_{x,y}$) directly correlates with an attractive state from the [$H_2O(^1B_1;1b_1 \rightarrow 3s)$ + $H(^2S)$] asymptote.

In $H_3O$ dissociating into ($H_2O$ + H) of the Figure 7, the ground Rydberg $H_3O$ radical diabatically dissociates into the first excited [$OH(A^2\Sigma^+)$ + $H_2(X^1\Sigma_g^+)$] and the ion-ion pair [$OH^+(X^3\Sigma^-)$ + $H_2^-(X^2\Sigma_u^+)$] asymptotes. In the second dissociation path, one electron also jumps from the $1\pi^3$ orbital of OH to the $1\sigma^*$ orbital of $H_2$. All potential energy curves emerging from the antibonding interaction of the ($OH^*$ + $H_2$) asymptotes are diabatically repulsive, while a potential energy curve emerging from the [$OH^+(X^3\Sigma^-)$ + $H_2^-(X^2\Sigma_u^+)$] asymptote is diabatically attractive. At shorter than $R_{(OH)}$ ≅1.8 Å, the avoided curve crossings between the dissociative diabatic states of [$(H_3O^+)(e^-)_{Rydberg}$] and the repulsive diabatic states from ($OH^*$ + $H_2$) are occurred. While, at larger than $R_{(OH)}$ ≅1.8 Å, the curve crossings between the diabatically attractive diabatic state of [$OH^+(X^3\Sigma^-)$ + $H_2^-(X^2\Sigma_u^+)$] and the diabatically repulsive diabatic states of ($OH^*$ + $H_2$) are found. As a result, two potential barriers in the $4^2A_1$ state are formed by two kinds of curve crossings. By the avoided curve crossings, the potential energy curve of the $4^2A_1$ state is bound between $R_{(OH)}$≅2.3 and 5.8 Å. Meanwhile, in the excited $2^2A_1$ and $3^2A_1$ states, a potential energy barrier is found at $R_{(OH)}$≅1.8 Å. That is, the barriers of the excited $2^2A_1$ and $3^2A_1$ states are coupled by strongly avoided curve crossings between strongly attractive ionic states emerging from ($OH^+$ + $H_2^-$) and the repulsive diabatic state from ($OH^*$ + $H_2$). For the $^2B_1$ states of $H_3O$ dissociating into (OH + $H_2$), the $1^2B_1$ state emerging from [$OH(X^2\Pi)$ + $H_2(X^1\Sigma_g^+)$] asymptote correlates to the $^2E$ excited state of $H_3O$. It is also made by an avoided curve crossing between the dissociative diabatic state of the Rydberg [$(H_3O^+)(e^-)_{Rydberg}$] radical and the repulsive diabatic state emerging from the ($OH^*$ + $H_2$) asymptote.

Adiabatic potential energy curves of the dissociation of $H_3O$ into ($H_2O$ + H) have been investigated by some groups.[44,46,49] According to their curves, the ground $^2A_1$ state surface along the OH bond rupture has a very low potential energy barrier. In the result of Luo and Jungen,[49] a barrier height is found to be ≅0.08 eV. Particularly, around $R_{(OH)}$ ≅3.0 Å, the curve is also bound shallowly. In the results of Niblaeus *et al.*,[46] a barrier of ≅0.13 eV is found at $R_{(OH)}$ ≅1.248 Å. The potential barrier is found to be sensitive to the diffuse basis set. They concluded that the origin of the barrier is a curve crossing between a repulsive state and an attractive Rydberg state. But, the avoided curve crossings have not been represented clearly.

Here, it is important thing to investigate the characteristically avoided curve crossings of the potential curves for the dissociation of $H_3O$ into its product asymptotes. The potential curves for the dissociation of [$(AH_a^+)(e^-)_{Rydberg}$] into its products are formed by two kinds of the avoided curve crossings. One is occurred between the dissociative diabatic states emerging from [$(AH_a^+)(e^-)_{Rydberg}$] and the repulsive diabatic states from ($AH_b^*$ + $H_c$). The other is occurred between the repulsive diabatic states emerging from ($AH_b^*$ + $H_c$) and the attractively ionic diabatic state from the ion-ion pair ($AH_b^+$ + $H_c^-$) asymptote. To understand the avoided curve crossing, we have analyzed the contributions of the dominant configuration to the total wave functions of the $^2A_1$ states and listed them in Table V and VI.

The dominant configuration for the ground $^2A_1$ state is [core]$2a_1^2\ 1e^4\ 3a_1^2\ 4a_1^1$ at the $H_3O$ structure, [core]$2a_1^2\ 1b_2^2\ 3a_1^2\ 1b_1^2\ (4a_1^1)_H$ at the ($H_2O$ + H) asymptote, and [core]$2\sigma^2\ 3\sigma^1\ 1\pi_x^2\ 1\pi_y^2\ (4\sigma^2)_{H2}$ at the (OH + $H_2$) asymptote. $2a_1^2\ 1e^4\ 3a_1^2$ is an electronic configuration of $H_3O^+$. $4a_1^1$ indicates an electron of the Rydberg 3s orbital having a $H_3O^+$ structure as a core. The electronic structure of $H_3O$ is represented to be $[(H_3O^+)(e^-)_{3s}]$. Along OH bond rupture, the $4a_1$ orbital is nonbonding, *i.e.*, a character of 1s of H. $4a_1^1$ indicates one electron in the 1s orbital of H. That is, the configuration of $2a_1^2\ 1e^4\ 3a_1^2\ (1s^1)_H$ at $R_{(OH)}$=10.0 Å indicates the antibonding pair [$H_2O(^1A_1)$ + $H(^2S)$] asymptote. As a result, the dominant configuration of the ground $^2A_1$ state interconnecting the $H_3O$ structure with the ($H_2O$ + H) asymptote does not change from short internuclear distance to long. Meanwhile, along OH-$H_2$ bond rupture, the $(4\sigma^2)_{H2}$ orbital is a bonding character of $1\sigma^2$ of $H_2$. 1e orbital of $H_3O$ separates into two orbitals ($1\pi_x$, $1\pi_y$) in OH. Therefore, the configuration of $2\sigma^2\ 3\sigma^1\ 1\pi_x^2\ 1\pi_y^2\ (4\sigma^2)_{H2}$ at $R_{(OH)}$=8.0 Å indicates the antibonding pair [$OH(A^2\Sigma^+)$ + $H_2(X^1\Sigma_g^+)$] asymptote.

For the dissociation of $H_3O$ into ($H_2O$ + H), the ground $(H_3O^+)(e^-)_{3s}$ radical diabatically correlates into the [$H_2O(^1A_1$; $1b_1 \rightarrow 3p_{x,y})$ + $H(^2S)$] and [$H_2O^+(^2A_1)$ + $H^-(^1S)$] asymptotes. In Table V, the dominant configurations of the [$H_2O(^1A_1$; $1b_1 \rightarrow 3p_{x,y})$ + $H(^2S)$] and [$H_2O^+(^2A_1)$ + $H^-(^1S)$] asymptotes are 22211001 and 22210002, respectively. In the diabatic dissociation of $H_3O$ into [$H_2O(^1A_1$; $1b_1 \rightarrow 3p_{x,y})$ + $H(^2S)$], the contribution for the configuration of 22211001 begins to appear the first excited $^2A_1$ state at $R_{(OH)}$=3.0 Å and the contribution of it increases with internuclear distance. From $R_{(OH)}$=5.0 Å it become a dominant configuration in the first $^2A_1$ state. In the diabatic dissociation of $H_3O$ into the ion-ion pair [$H_2O^+(^2A_1)$ + $H^-(^1S)$] asymptote, the contribution for the configuration of 22210002 represents the first excited $^2A_1$ state from $R_{(OH)}$=2.2 Å to 4.0 Å. Around $R_{(OH)}$=4.0 Å, the contribution represents the second excited $^2A_1$ state. This configuration can be strongly attractive ion character as an ion approaches to the other. Two attractive diabatic characters greatly influence the curve crossing, that is, the contributions of those characters are larger than that of the repulsive character. As the result, the potential energy barrier of the ground $^2A_1$ state is shifted to the equilibrium geometry of $H_3O$. And the barrier height appears to be low.

In the excited $2^2A_1$ state, the dominant configuration is $2a_1^2\ 1e^4\ 3a_1^2\ (3p_z)^1_{Rydberg}$ at shorter than $R_{(OH)} \cong 1.1$ Å, $2a_1^2\ 1b_2^2\ 3a_1^2\ 1b_1^2\ (3p_z)^1_{Rydberg}$ between $R_{(OH)} \cong 1.2$ and $\cong 2.1$ Å, $2a_1^2\ 1b_2^2\ 3a_1^2\ 1b_1^1\ (1s)^2_H$ between $R_{(OH)} \cong 2.2$ and $\cong 4.5$ Å, and $2a_1^2\ 1b_2^2\ 3a_1^2\ 1b_1^1\ (3p_{x,y})^1_{Rydberg}\ (1s)^1_H$ at larger than $R_{(OH)} \cong 4.5$ Å. In the dissociation of $H_3O$ into ($H_2O$ + H), $2a_1^2\ 1e^4\ 3a_1^2\ (3p_z)^1_{Rydberg}$ at shorter than $R_{(OH)} \cong 1.1$ Å represents the $(H_3O^+)(e^-)3p_z$ structure, $2a_1^2\ 1b_2^2\ 3a_1^2\ 1b_1^2\ (3p_z)^1_{Rydberg}$ between $R_{(OH)} \cong 1.2$ and $\cong 2.1$ Å represents $(H_2O \ldots H^+)(e^-)3p_z$, $2a_1^2\ 1b_2^2\ 3a_1^2\ 1b_1^1\ (1s)^2_H$ between $R_{(OH)} \cong 2.2$ and $\cong 4.5$ Å represents $(H_2O^+ \ldots H^-)$, and $2a_1^2\ 1b_2^2\ 3a_1^2\ 1b_1^1\ (3p_{x,y})^1_{Rydberg}\ (1s)^1_H$ at larger than $R_{(OH)} \cong 4.5$ Å represents $[(H_2O^+)(e^-)3p_{x,y} + H]$. More interestingly, the $2^2A_1$ state between $R_{(OH)} \cong 2.2$ and $\cong 4.5$ Å has a dominant configuration of $2a_1^2\ 1b_2^2\ 3a_1^2\ 1b_1^1\ (1s)^2_H$ which means an ion-ion interaction structure as $(H_2O^+ \ldots H^-)$. Here one electron jumped from the Rydberg $3p_z$ orbital of $H_2O$ to the 1s orbital of H.

The dominant configuration of the $3^2A_1$ state is $2a_1^2\ 1e^4\ 3a_1^2\ (4s)^1_{Rydberg}$ at shorter than $R_{(OH)} \cong 1.1$ Å, $2a_1^2\ 1b_2^2\ 3a_1^2\ 1b_1^2\ (3p_z)^1_{Rydberg}$ between $R_{(OH)} \cong 1.2$ and $\cong 2.1$ Å, $2a_1^2\ 1b_2^2\ 3a_1^2\ 1b_1^1\ (3p_{x,y})^1_{Rydberg}\ (1s)^1_H$ between $R_{(OH)} \cong 2.2$ and $\cong 3.8$ Å, $2a_1^2\ 1b_2^2\ 3a_1^2\ 1b_1^1\ (1s)^2_H$ between $R_{(OH)} \cong 3.8$ and $\cong 4.5$ Å, and $2a_1^2\ 1b_2^2\ 3a_1^2\ 1b_1^1\ (3p_{x,y})^1_{Rydberg}\ (1s)^1_H$ at larger than $R_{(OH)} \cong 4.5$ Å. In the electronic structure, $2a_1^2\ 1e^4\ 3a_1^2\ (4s)^1_{Rydberg}$ represents $(H_3O^+)(e^-)_{4s}$, $2a_1^2\ 1b_2^2\ 3a_1^2\ 1b_1^2\ (3p_z)^1_{Rydberg}$ represents $[(H_2O) \ldots (H^+)](e^-)3p_z$, $2a_1^2\ 1b_2^2\ 3a_1^2\ 1b_1^1\ (1s)^2_H$ represents $(H_2O^+ \ldots H^-)$, and $2a_1^2\ 1b_2^2\ 3a_1^2\ 1b_1^1\ (3p_{x,y})^1_{Rydberg}\ (1s)^1_H$ represents $[(H_2O^+)(e^-)_{3s} + H]$. Around $R_{(OH)} \cong 4.0$ Å, the dominant configuration represents $2a_1^2\ 1b_2^2\ 3a_1^2\ 1b_1^1\ (1s)^2_H$ which means the attractive interaction of $[H_2O^+ \ldots H^-]$. The changes of these configurations are in accordance with the potential energy curves in Figure 6.

For the dissociation of $H_3O$ into ($OH$ + $H_2$), the ground $^2A_1$ state of the $(H_3O^+)(e^-)_{3s}$ radical diabatically correlates into the $[OH(^4\Sigma^-) + H_2(X^1\Sigma_g^+)]$ and $[OH^+(X^3\Sigma^-) + H_2^-(X^2\Sigma_u^+)]$ asymptotes. The dominant configurations of $[OH(^4\Sigma^-) + H_2\ (X^1\Sigma_g^+)]$ and $[OH^+(X^3\Sigma^-) + H_2^-(X^2\Sigma_u^+)]$ are 221112 as a [core] $2\sigma^2\ 3\sigma^2\ 1\pi_x^1\ 1\pi_y^1\ 4\sigma^1\ (1\sigma^2)_{H2}$ configuration and 221121 as [core] $2\sigma^2\ 3\sigma^2\ 1\pi_x^1\ 1\pi_y^1\ [(1\sigma)^2\ (1\sigma^*)^1]_{H2}$, respectively. In diabatic dissociation of $H_3O$ into $[OH(^4\Sigma^-) + H_2\ (X^1\Sigma_g^+)]$, the contribution for the configuration of 221112 begins to appear the $2^2A_1$ state at $R_{(OH)}$=2.1 Å and the contribution of it increases with internuclear distance. In diabatic dissociation of $H_3O$ into $[OH^+(X^3\Sigma^-) + H_2^-(X^2\Sigma_u^+)]$, the contribution for the configuration of 221121 represents the $2^2A_1$ state from $R_{(OH)}$=1.5 to 2.0 Å. This configuration can be strongly attractive ion character as an ion approaches to the other. The attractive diabatic character greatly influences on the curve crossing, that is, the contribution of this character is larger than that of the repulsive character.

In the excited $2^2A_1$ state, the dominant configuration is $2a_1^2\ 1e^4\ 3a_1^2\ (3p_z)^1_{\mathrm{Rydberg}}$ at shorter than $R_{(OH)}\cong 1.1$ Å, $2\sigma^2\ 3\sigma^2\ 1\pi_x^1\ 1\pi_y^1\ (4\sigma)^2\ (3p_z)^1_{\mathrm{Rydberg}}$ between $R_{(OH)}\cong 1.2$ and $\cong 1.5$ Å, $2\sigma^2\ 3\sigma^2\ 1\pi_x^1\ 1\pi_y^1\ [(1\sigma)^2\ (1\sigma^*)^1]_{H2}$ between $R_{(OH)}\cong 1.5$ and $\cong 2.0$ Å, and $2\sigma^2\ 3\sigma^2\ 1\pi_x^1\ 1\pi_y^1\ 4\sigma^1\ (1\sigma^2)_{H2}$ at larger than $R_{(OH)}\cong 2.1$ Å. That is, at shorter than $R_{(OH)}\cong 1.1$ Å, $2a_1^2\ 1e^4\ 3a_1^2\ (3p_z)^1_{\mathrm{Rydberg}}$ represents the $(H_3O^+)(e^-)_{3pz}$ structure, $2\sigma^2\ 3\sigma^2\ 1\pi_x^1\ 1\pi_y^1\ (4\sigma)^2\ (3p_z)^1_{\mathrm{Rydberg}}$ between $R_{(OH)}\cong 1.2$ and $\cong 1.5$ Å represents $(HO\ldots H_2)^+(e^-)3p_z$, $2\sigma^2\ 3\sigma^2\ 1\pi_x^1\ 1\pi_y^1\ [(1\sigma)^2\ (1\sigma^*)^1]_{H2}$ between $R_{(OH)}\cong 1.5$ and $\cong 2.0$ Å represents $(HO^+\ldots H_2^-)$, and $2\sigma^2\ 3\sigma^2\ 1\pi_x^1\ 1\pi_y^1\ 4\sigma^1\ (1\sigma^2)_{H2}$ at larger than $R_{(OH)}\cong 2.1$ Å represents $[OH(^4\Sigma^-) + H_2(X^1\Sigma_g^+)]$. More interestingly, the $2^2A_1$ state between $R_{(OH)}\cong 1.5$ and $\cong 2.0$ Å has a dominant configuration of $2\sigma^2\ 3\sigma^2\ 1\pi_x^1\ 1\pi_y^1\ [(1\sigma)^2\ (1\sigma^*)^1]_{H2}$ which means an ion-ion interaction structure as $(HO^+\ldots H_2^-)$. Here one electron jumped from the Rydberg $3p_z$ orbital of OH to the $[(1\sigma^*)^1]_{H2}$ orbital of $H_2$. Therefore, this state has strongly attractive ion character. The changes of these configurations are in accordance with the potential energy curves in Figure 7.

As shown in Figure 6 and 7, in the $H_3O$ radical dissociating into ($H_2O$ + H), the potential energy barrier is formed by two avoided curve crossings between two attractive diabatic states emerging from $[H_2O(^1A_1;1b_1\rightarrow 3p_{x,y}) + H(^2S)]$ and $[H_2O^+(^2A_1) + H^-(^1S)]$ and a repulsive state from an antibonding interaction of $[H_2O(^1A_1) + H(^2S)]$. Two attractive characters from $[H_2O(^1A_1;\ 1b_1\rightarrow 3p_{x,y}) + H(^2S)]$ and $[H_2O^+(^2A_1) + H^-(^1S)]$ greatly influence on the curve crossing. In the $H_3O$ radical dissociating into ($OH$ + $H_2$), the ground $^2A_1$ state of the Rydberg $H_3O$ radical diabatically dissociates into the $[OH(^4\Sigma^-) + H_2(X^1\Sigma_g^+)]$ and $[OH^+(X^3\Sigma^-) + H_2^-(X^2\Sigma_u^+)]$ asymptotes. When the internuclear distance between $OH^+$ and $H_2^-$ become short, the attractive state emerging from the ion-ion pair diabatically correlates with $H_3O$. This state is diabatically bound due to the ion-ion electrostatic attraction. As a result, the maximum position of the ground potential barrier formed by the avoided curve crossing is located out of line of those of the excited potential energy curves.

**Table I**. Bond lengths (Å) and relative energies (eV) for the $NH_4$ radical dissociating into ($NH_3$ + H) and ($NH_2$ + $H_2$). Ionization and excitation energies (eV) of $NH_4$, $NH_3$, and $NH_2$. The numbers in parentheses indicate the vertical ionization energy.

| | SECI$^{a}$ | SDCI$^{a}$ | MP2$^{b}$ | CCSD(t)$^{b}$ | CIPSI$^{c}$ | | SDCI$^{d}$ | | exptl$^{e}$ |
|---|---|---|---|---|---|---|---|---|---|
| $^{2}A_1$ state emerging from ($NH_3$ + H) | | | | | | | | | |
| $R_{(NH)eq}$ | 1.022 | 1.040 | 1.034 | 1.040 | 1.033 | | 1.041 | | |
| $R_{(NH)TS}$ | 1.339 | 1.439 | 1.411 | 1.425 | 1.369 | | 1.427 | | |
| $\Delta E_{(NH4\text{-}TS)}$ | 0.75 | 0.83 | 0.77 | 0.79 | 0.88 | | 0.85 | | |
| $\Delta E_{[TS\text{-}(NH3+H)]}$ | 0.59 | 0.61 | 0.60 | 0.57 | 0.52 | | 0.64 | | |
| $\Delta E_{[NH4\text{-}(NH3+H)]}$ | -0.17 | -0.22 | -0.20 | -0.22 | -0.23 | | -0.21 | | -0.3 |
| $^{2}A_1$ state emerging from ($NH_2$ + $H_2$) | | | | | | | | | |
| $R_{(NH)eq}$ | | 1.039 | 1.036 | 1.040 | 1.033 | | 1.041 | | |
| $R_{(NH)TS}$ | | 1.590 | | | | | | | |
| $\Delta E_{(TS\text{-}NH4)}$ | | 3.59 | | | | | | | |
| $\Delta E_{[TS\text{-}(NH2+H2)]}$ | | 1.06 | | | | | | | |
| $\Delta E_{[NH4\text{-}(NH2+H2)]}$ | | -2.53 | | | | | | | |
| $^{2}B_1$ state emerging from ($NH_2$ + $H_2$) | | | | | | | | | |
| $\Delta E_{eq}$ | | 1.015 | | | | | | | |
| $\Delta E_{TS}$ | | 1.590 | | | | | | | |
| $\Delta E_{(TS\text{-}NH4)}$ | | 2.96 | | | | | | | |
| $\Delta E_{[TS\text{-}(NH2+H2)]}$ | | 4.66 | | | | | | | |
| $\Delta E_{[NH4\text{-}(NH2+H2)]}$ | | -1.69 | | | | | | | 0.32 |
| $NH_4$ | | | | | | | | | |
| I.E.$^{f}$ | 4.52 | 4.57 | 4.58 | 4.60 | | | 4.85$^{g}$ | | 4.62$^{h}$,4.73$^{i}$ |
| $\Delta E_{(3s\text{-}3p)}$ | 1.55 | 1.90 | | | 1.66 | | 1.89 | | |
| $\Delta E_{(3s\text{-}4s)}$ | 2.46 | 2.66 | | | 2.65 | | | | |
| $\Delta E_{(3s\text{-}3d)}$; $^{2}T_2$ | 2.61 | 2.85 | | | | | 2.89 | | 2.19$^{j}$ |
| $\Delta E_{(3s\text{-}3d)}$; $^{2}E$ | 2.69 | 2.93 | | | | | 3.04 | | |
| $\Delta E_{(3s\text{-}4p)}$ | 2.90 | 3.15 | | | | | | | |
| $\Delta E_{(3s\text{-}5s)}$ | 3.22 | 3.45 | | | | | | | |
| $\Delta E_{(3s\text{-}4d)}$; $^{2}T_2$ | 3.29 | 3.53 | | | | | | | |
| $\Delta E_{(3s\text{-}4d)}$; $^{2}E$ | 3.32 | 3.61 | | | | | | | |
| $\Delta E_{(3p\text{-}3d)}$; $^{2}T_2$ | 1.06 | 1.23 | | | | | | | 1.87$^{j}$ |
| $NH_3$ | | | | | | | | | |
| I.E.$^{f}$ | 10.02 | 10.13 | 10.10 | 10.14 | | | | | 10.17$^{l}$ |
| P.A.$^{k}$ | 9.18 | 9.22 | 9.23 | 9.24 | 9.58$^{m}$ | | 9.23$^{n}$ | | |
| $\Delta E_{(n\text{-}3s)}$; $A^{3}A_1$ | 6.46 | 6.31 | | | | | 6.27$^{o}$ | | 6.38$^{l}$ |
| $\Delta E_{(n\text{-}3px,y)}$; $B^{3}E$ | 7.88 | 7.86 | | | | 7.84$^{o}$ | | 7.90$^{l}$ | |
| $\Delta E_{(n\text{-}3pz)}$; $^{3}A_1$ | 8.29 | 8.05 | | | | 7.84$^{o}$ | | 8.14$^{l}$ | |
| $\Delta E_{(n\text{-}4s)}$; $^{3}A_1$ | 8.98 | 9.06 | | | | | | | 9.11$^{l}$ |
| $\Delta E_{(n\text{-}3d)}$; $^{3}E$ | 9.09 | 9.23 | | | | | | | |
| $NH_2$ | | | | | | | | | |
| I.E.$^{p}$ | | 11.0(11.77)$^{r}$ | | 11.20$^{s}$(11.37)$^{t}$ | | 10.9$^{u}$ | 11.14$^{v}$ | 11.46(12.00)$^{t}$ | |
| I.E.$^{q}$ | | 12.16(12.22)$^{r}$ | | 12.48$^{s}$(12.10)$^{t}$ | | | 12.45$^{v}$ | 12.45(12.45)$^{t}$ | |
| $\Delta E_{(12B1\text{-}12A1)}$ | 2.22 | 2.20$^{w}$ | | | 2.26$^{y}$ | 2.16$^{z}$ | | | |
| $\Delta E_{(12B1\text{-}12B2)}$ | 6.58 | 6.50$^{w}$ | | | 6.50$^{y}$ | 6.64$^{z}$ | | | |

**(continued Table I)**

| | SECI[a] | SDCI[a] | MP2[b] | CCSD(t)[b] | CIPSI[c] | SDCI[d] | exptl[e] |
|---|---|---|---|---|---|---|---|
| $\Delta E_{(12B1\text{-}22A1)}$ | 7.59 | 7.55[w] | | 7.74[x] | 7.77[y] | 7.69[z] | |
| $\Delta E_{(12B1\text{-}22B1)}$ | 7.65 | 7.62[w] | | 7.70[x] | 7.49[y] | 7.63[z] | |
| $\Delta E_{(12B1\text{-}32B1)}$ | 9.46 | 9.38[w] | | 9.45[x] | 9.57[y] | 9.46[z] | |
| $\Delta E_{(12B1\text{-}42B1)}$ | 9.69 | 9.43[w] | | 9.76[x] | | | |
| $\Delta E_{(12B1\text{-}32A1)}$ | 9.80 | 9.61[w] | | 10.06[x] | | | |
| $\Delta E_{(12B1\text{-}52B1)}$ | 9.87 | 9.83[w] | | 9.83[x] | | | |
| $\Delta E_{(12B1\text{-}42A1)}$ | 9.90 | 9.87[w] | | 9.89[x] | | | |
| $\Delta E_{(12B1\text{-}62B1)}$ | 10.29 | 10.18[w] | | 10.08[x] | | | |
| $\Delta E_{(12B1\text{-}52A1)}$ | 10.48 | 10.46[w] | | 11.51[x] | | | |
| $\Delta E_{(12B1\text{-}72B1)}$ | 11.64 | 11.49[w] | | 11.42[x] | | | |
| $\Delta E_{(12B1\text{-}62A1)}$ | 11.68 | 11.59[w] | | | | | |
| $\Delta E_{(12B1\text{-}72A1)}$ | 12.17 | 12.21[w] | | | | | |

[a] SECI and SDCI energies were obtained with the MOs and geometries of $NH_4^+$ calculated by RHF at each internuclear distance. [b] CCSD(t) energies were obtained with Gaussian 98. [c] Reference 22. [d] Reference 23. [e] Cited from reference 22. [f] Ionization energies of $NH_4$ and $NH_3$. [g] Reference 27. [h] Reference 4. [i] Reference 11. [j] Reference 5. [k] Proton affinity of $NH_3$. [l] Reference 70. [m] Reference 30. [n] Reference 71. [o] Reference 72. [p] Adiabatic ionization energy of $X^3B_1$ of $NH_2^+$ from $X^2A_1$ of $NH_2$. [q] Adiabatic ionization energy of $A^1A_1$ of $NH_2^+$ from $X^2A_1$ of $NH_2$. [r] Reference 73. [s] Reference 74. [t] Reference 75. [u] Reference 76. [v] Reference 77. [w] Reference 78. [x] Reference 79. [y] Reference 80. [z] Reference 81.

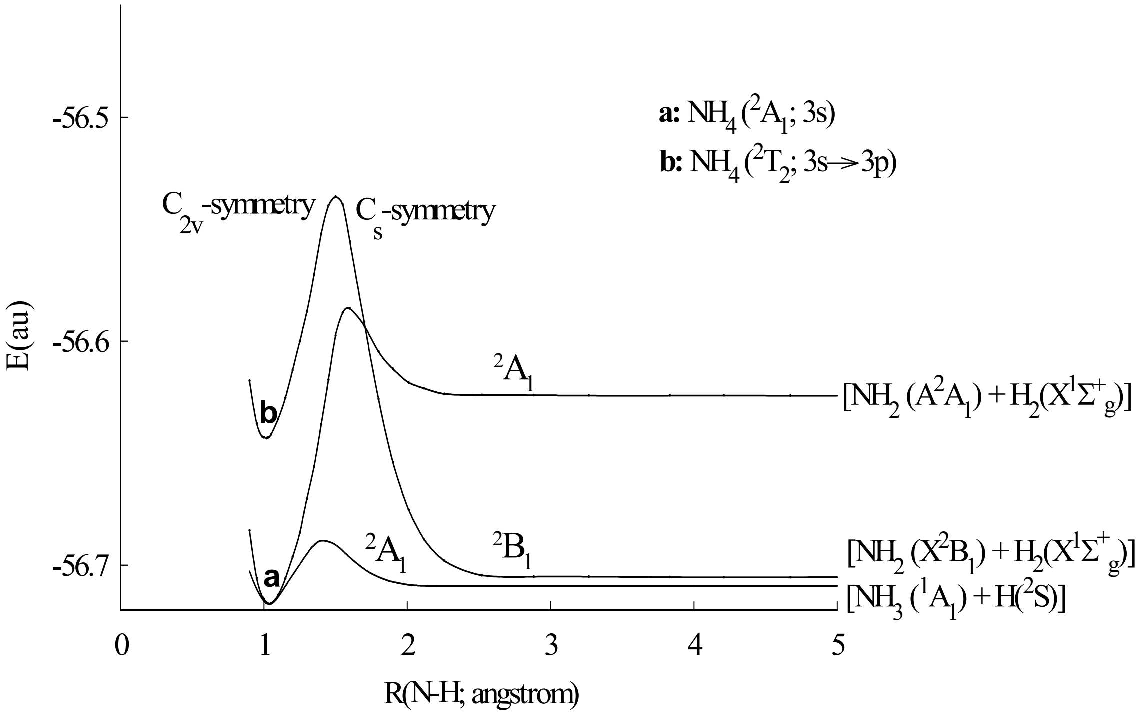

Figure 1. Potential energy curves for the $^2A_1$ and $^2B_1$ states of the Rydberg $NH_4$ radical dissociating into ($NH_3$ + H) and ($NH_2$ + $H_2$) obtained with the SDCI level.

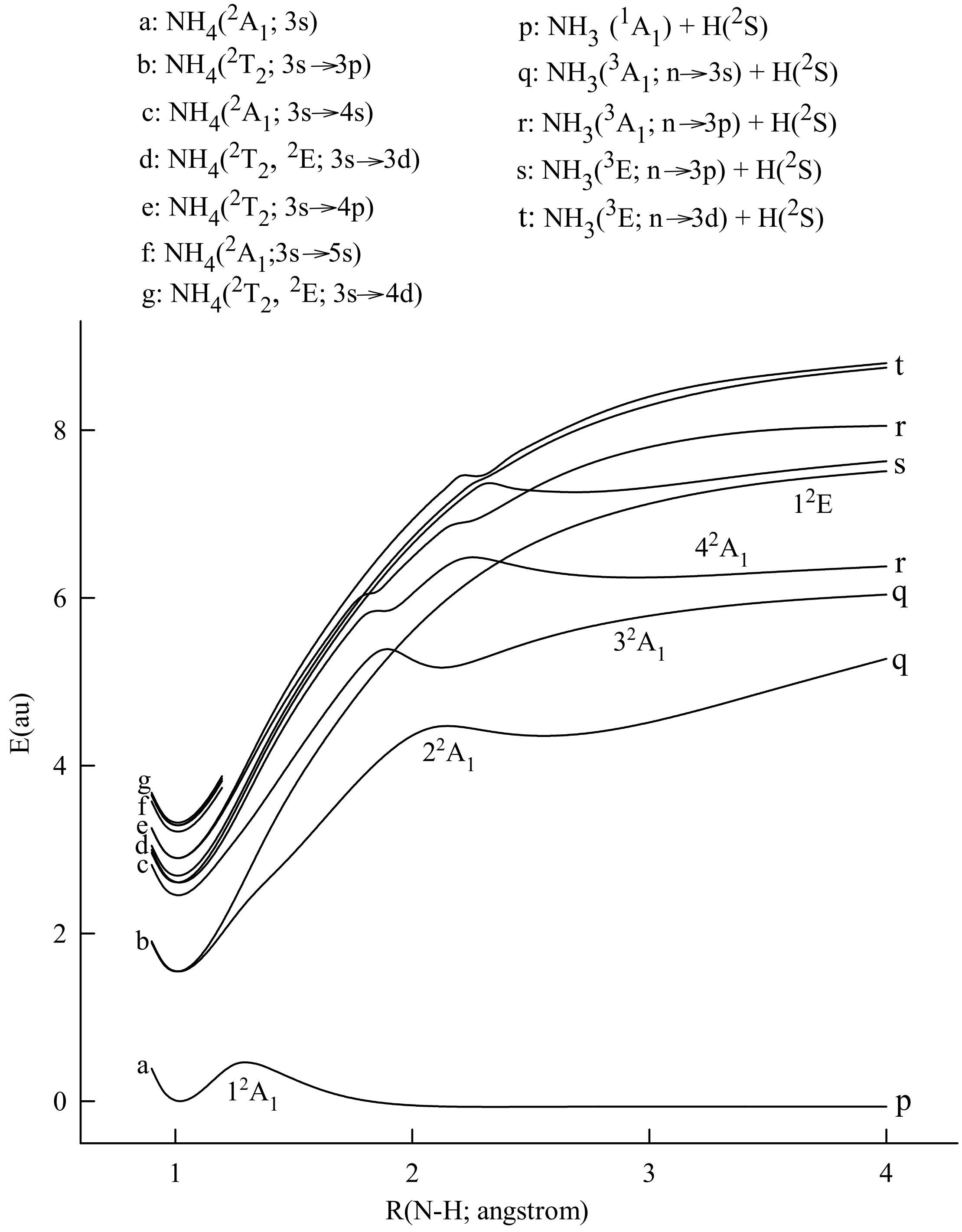

Figure 2. Adiabatic potential energy curves for the ground and excited states of the Rydberg $NH_4$ radical dissociating into ($NH_3$ + H)

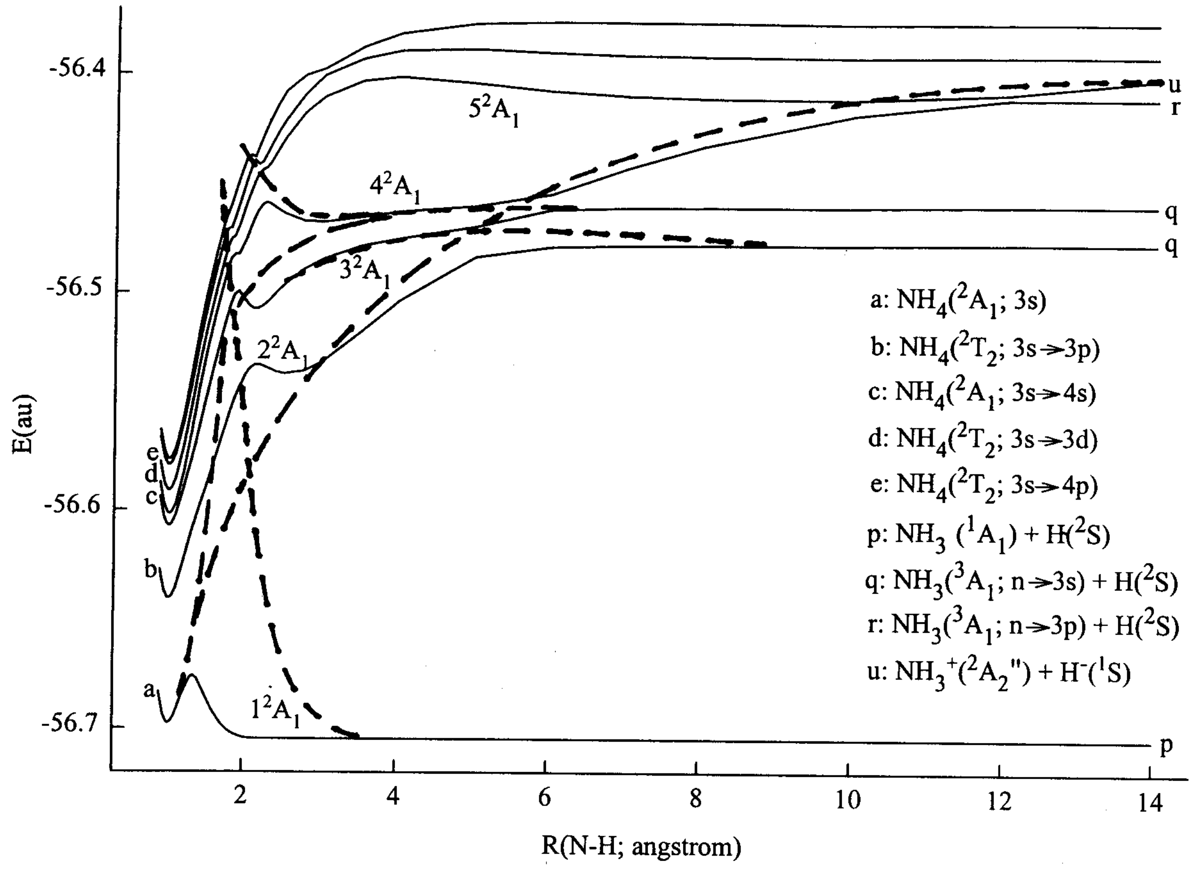

Figure 3. Avoided curve crossings for the $^2A_1$ states of the Rydberg $NH_4$ radical dissociating into ($NH_3$ + H). Broken lines indicate estimated diabatic potential curves.

**Table II**. Contributions of the dominant configuration for the low lying Rydberg $^2A_1$ states along the $NH_4$ radical dissociating into ($NH_3$ + H). 222210 denotes $2a_1^2\ 1t_1^6\ 3a_1^1\ 4a_1^0$ configuration.

| $R_{(NH)}$(Å) | $1^2A_1$ | $2^2A_1$ | $3^2A_1$ | $4^2A_1$ |
|---|---|---|---|---|
| 0.9 | 22221 0.9983 | 22220001 0.9989 | 222200001 0.9997 | 222200000001 0.9998 |
| 1.0 | 22221 0.9982 | 22220001 0.9986 | 222200001 0.9997 | 222200000001 0.9997 |
| 1.1 | 22221 0.9977 | 22220100 0.9978 | 222200001 0.9993 | 222200000100 0.9992 |
| 1.2 | 22221 0.9962 | 22220100 0.9954 | 222200001 0.9972 | 222200000100 0.9984 |
| 1.4 | 22221 0.9857 | 22220100 0.9827 | 222200001 0.9914 | 222200000100 0.9959 |
| 1.5 | 22221 0.9801 | 22220100 0.9771<br>22211100 0.0319<br>22212000 0.0861 | 222200001 0.9986 | 222200000100 0.9901 |
| 1.6 | 22221 0.9760 | 22220100 0.9681<br>22211100 0.0820<br>22212000 0.1056 | 222200001 0.9837 | 222200000100 0.9794 |
| 1.8 | 22221 0.9692 | 22220100 0.9322<br>22211100 0.1475<br>22212000 0.1740 | 222200001 0.9261 | 222200000100 0.8419 |
| 2.0 | 22221 0.9631 | 22220100 0.8301<br>22211100 0.2357<br>22212000 0.3679 | 222120000 0.7155 | 222200001000 0.8618 |
| 2.1 | 22221 0.9600 | 22220100 0.6953<br>22211100 0.2807<br>22212000 0.5426 | 222120000 0.6190 | 222200001000 0.8343 |
| 2.2 | 22221 0.9568 | 22212000 0.6818<br>22211100 0.3015 | 222201000 0.6599 | 222200001000 0.6794 |
| 2.3 | 22221 0.9537 | 22212000 0.7450<br>22211100 0.3064 | 222201000 0.7056 | 222111000000 0.6523 |
| 2.5 | 22221 0.9480 | 22212000 0.7775<br>22211100 0.3139 | 222201000 0.6856 | 222111000000 0.6997 |
| 3.0 | 22221 0.9391 | 22212000 0.7646<br>22211100 0.3537 | 222201000 0.5295 | 222111000000 0.6870 |
| 3.5 | 22221 0.9379 | 22212000 0.7375<br>22211100 0.4031 | 222201000 0.3814 | 222111000000 0.6525 |
| 4.0 | 22221 0.9397 | 22212000 0.7009<br>22211100 0.4500 | 222120000 0.4036 | 222110100000 0.5200 |
| 5.0 | 22221 0.9425 | 22211100 0.4915 | 222120000 0.5805 | 222110100000 0.6064 |
| 6.0 | 22221 0.9437 | 22211010 0.5458 | 222110100 0.6164 | 222120000000 0.7491 |
| 7.0 | 22221 0.9444 | 22211010 0.5709 | 222110100 0.6865 | 222120000000 0.7970 |
| 8.0 | 22221 0.9450 | 22211010 0.5720 | 222110100 0.6923 | 222120000000 0.8065 |
| 10.0 | 22221 0.9462 | 22211010 0.5517 | 222110100 0.6715 | 222120000000 0.8168 |
| 12.0 | 22221 0.9468 | 22211010 0.5298 | 222110100 0.6474 | 222110100000 0.6138 |
| 14.0 | 22221 0.9473 | 22211010 0.5151 | 222110100 0.6299 | 222110100000 0.6522 |

a: $NH_4$ ($^2A_1$; 3s)
b: $NH_4$ ($^2T_2$; 3s $\rightarrow$ 3p)
c: $NH_4$ ($^2A_1$; 3s $\rightarrow$ 4s)
d: $NH_4$ ($^2T_2$, $^2E$; 3s $\rightarrow$ 3d) ,
e: $NH_4$ ($^2T_2$; 3s $\rightarrow$ 4p)

p: $NH_2$ ($1^2B_1$) + $H_2(X^1\Sigma^+_g)$
q: $NH_2$ ($1^2A_1$) + $H_2(X^1\Sigma^+_g)$

r: $NH_2$ ($2^2A_1$) + $H_2(X^1\Sigma^+_g)$
s: $NH_2$ ($3^2A_1$) + $H_2(X^1\Sigma^+_g)$
t: $NH_2$ ($4^2A_1$) + $H_2(X^1\Sigma^+_g)$
u: $NH_2$ ($5^2A_1$) + $H_2(X^1\Sigma^+_g)$
v: $NH_2$ ($6^2A_1$) + $H_2(X^1\Sigma^+_g)$
w: $NH_2$ ($7^2A_1$) + $H_2(X^1\Sigma^+_g)$
x: $NH_2^+(A^1A_1)$ + $H_2^-(X^2\Sigma^+_u)$

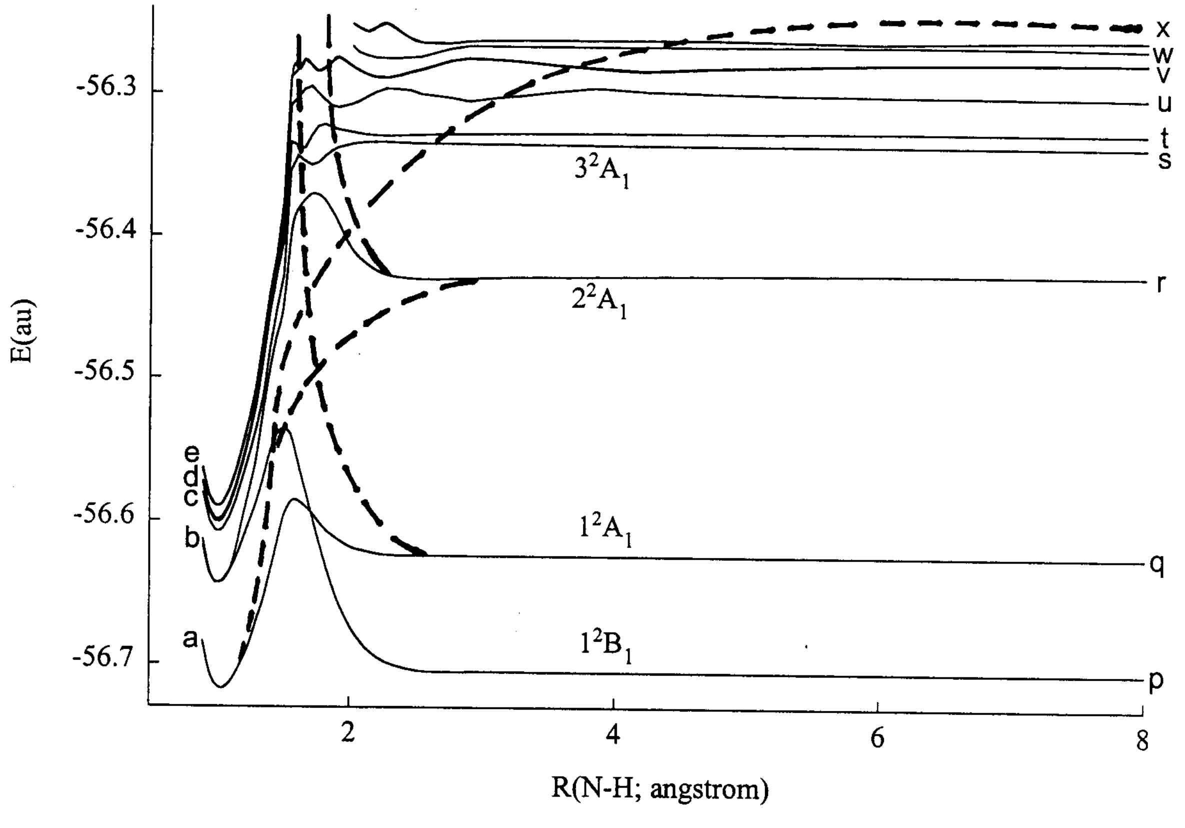

Figure 4. Avoided curve crossings for the $^2A_1$ states of the Rydberg $NH_4$ radical dissociating into ($NH_2$ + $H_2$). Broken lines indicate estimated diabatic potential curves.

**Table III**. Contributions of the dominant configuration for the low lying Rydberg $^2A_1$ states along the $NH_4$ radical dissociating into ($NH_2 + H_2$). 222210 denotes $2a_1^2\ 1t_1^6\ 3a_1^1\ 4a_1^0$ configuration.

| $R_{(NH)}$(Å) | $1^2A_1$ | | $2^2A_1$ | | $3^2A_1$ | |
|---|---|---|---|---|---|---|
| 0.9 | 222210 | 0.9987 | 22220001 | 0.9989 | 222200001 | 0.9897 |
| 1.0 | 222210 | 0.9981 | 22220001 | 0.9982 | 222200001 | 0.9853 |
| 1.1 | 222210 | 0.9976 | 22220001 | 0.9878 | 222200001 | 0.9834 |
| 1.2 | 222210 | 0.9960 | 22120200 | 0.9954 | 221202000 | 0.6798 |
| 1.4 | 222210 | 0.9872 | 22120200 | 0.9827 | 221202000 | 0.6972 |
| 1.5 | 222210 | 0.9753 | 22202100 | 0.5978 | 222012000 | 0.5596 |
| | | | 22201200 | 0.0861 | | |
| 1.6 | 222102 | 0.9892 | 22202100 | 0.5788 | 222012000 | 0.5982 |
| | | | 22201200 | 0.1056 | | |
| 1.8 | 222102 | 0.9914 | 22202100 | 0.5523 | 222002100 | 0.6056 |
| | | | 22201200 | 0.2475 | | |
| 2.0 | 221202 | 0.8848 | 22202100 | 0.5311 | 222002100 | 0.6937 |
| | | | 22201200 | 0.4357 | | |
| 2.1 | 221202 | 0.9105 | 22201200 | 0.6653 | 222002100 | 0.7298 |
| 2.2 | 221202 | 0.9289 | 22201200 | 0.6818 | 222002100 | 0.7677 |
| 2.3 | 221202 | 0.9493 | 22201200 | 0.7450 | 222002100 | 0.7993 |
| 2.5 | 221202 | 0.9546 | 22201200 | 0.7775 | 222012000 | 0.8579 |
| 3.0 | 221202 | 0.9633 | 22201200 | 0.8273 | 222012000 | 0.8992 |
| 3.5 | 221202 | 0.9686 | 22201200 | 0.8976 | 222012000 | 0.9215 |
| 4.0 | 221202 | 0.9720 | 22201200 | 0.9380 | 222012000 | 0.9249 |
| 5.0 | 221202 | 0.9731 | 22201200 | 0.9542 | 222012000 | 0.9308 |
| 6.0 | 221202 | 0.9739 | 22201200 | 0.9583 | 222012000 | 0.9394 |
| 7.0 | 221202 | 0.9746 | 22201200 | 0.9606 | 222012000 | 0.9417 |
| 8.0 | 221202 | 0.9751 | 22201200 | 0.9706 | 222012000 | 0.9426 |

**Table IV**. Bond lengths (Å), angle (degree), and relative energies (eV) for the $H_3O$ radical dissociating into ($H_2O$ + H) and (OH + $H_2$). Ionization and excitation energies (eV) of $H_3O$, $H_2O$, OH, and $H_2$.

| | HF | SECI$^a$ | SDCI$^a$ | MP2$^b$ | CCSD(t)$^b$ | | HF$^c$ | CI$^d$ | CEPA$^e$ | exptl |
|---|---|---|---|---|---|---|---|---|---|---|
| $X^2A_1$ state emerging from ($H_2O$ + H) | | | | | | | | | | |
| $R_{(OH)eq}$ | 0.984 | 0.984 | 1.018 | 1.021 | 1.020 | | 0.984 | 1.053 | 1.02 | |
| $(\angle HOH)_{eq}$ | 107.6 | 106.3 | 106.0 | 105.7 | 105.9 | | 111.8 | 101.8 | 106.9 | |
| $R_{(OH)TS}$ | 1.174 | 1.122 | 1.213 | 1.215 | 1.210 | | 1.21 | 1.248 | | |
| $\Delta E_{(H3O-TS)}$ | 0.19 | 0.13 | 0.12 | 0.11 | 0.11 | | 0.29 | 0.13 | 0.08 | |
| $\Delta E_{[TS-(H2O+H)]}$ | 1.45 | 1.07 | 0.97 | 1.01 | 0.93 | | 1.51 | 1.02 | 1.08 | |
| $\Delta E_{[H3O-(H2O+H)]}$ | -1.27 | -0.94 | -0.86 | -0.90 | -0.82 | | -1.22 | -0.89 | -1.0 | |
| $X^2A_1$ state emerging from (OH + $H_2$) | | | | | | | | | | |
| $R_{(OH)eq}$ | 1.009 | 1.026 | 1.031 | 1.021 | 1.020 | | 0.984 | 1.053 | 1.02 | |
| $R_{(OH)TS}$ | 1.467 | 1.510 | 1.513 | | | | 1.248 | | | |
| $\Delta E_{(H3O-TS)}$ | | 5.24 | 4.99 | | | | | 0.13$^f$ | 0.08$^f$ | |
| $\Delta E_{[TS-(OH+H2)]}$ | 1.27 | 1.14 | | | | | 1.02$^f$ | 1.08$^f$ | | |
| $\Delta E_{[H3O-(OH+H2)]}$ | | -3.97 | -3.85 | | | | | -0.89$^f$ | -1.0$^f$ | |
| $A^2B_1$ state emerging from (OH + $H_2$) | | | | | | | | | | |
| $R_{(OH)eq}$ | | 1.014 | 1.019 | | | | | | | |
| $R_{(OH)TS}$ | 1.492 | 1.501 | | | | | | | | |
| $\Delta E_{(H3O-TS)}$ | | 5.11 | 5.02 | | | | | | | |
| $\Delta E_{[TS-(OH+H2)]}$ | | 7.36 | 7.18 | | | | | | | |
| $\Delta E_{[H3O-(OH+H2)]}$ | | -2.24 | -2.15 | | | | | | | |
| $H_3O$ | | | | | | | | | | |
| I.E.$^g$ | 4.73 | 4.95 | 5.30 | 5.32 | 5.34 | | 5.36 | 4.68$^h$ | 5.36 | 4.34$^k$ |
| | | | | | | 4.30$^i$ | 4.43$^j$ | 4.4$^l$ | | |
| | | | | | | 4.17$^i$ | | | | |
| $\Delta E_{(3s-3p)}$;$^2A_1$,$^2E$ | 2.09 | 1.92 | | | | | | 1.87$^h$ | 2.65 | 1.7$^k$ |
| $\Delta E_{(3s-4s)}$;$^2A_1$ | | 2.72 | 2.80 | | | | | | 3.18 | |
| $\Delta E_{(3s-3d)}$;$^2A_1$ | 2.99 | 3.04 | | | | | 3.71 | | | |
| $H_2O$ | | | | | | | | | | |
| I.E.$^g$ | 11.06 | 12.50 | 12.54 | 12.56 | 12.52 | | | 12.63$^n$ | | 12.6$^{p,q}$ |
| P.A.$^m$ | 7.60 | 7.44 | 7.32 | 7.39 | 7.30 | | | 7.45$^n$ | 7.22 | 7.18$^p$ |
| | | | | | 7.79$^o$ | 7.13 | | | | |
| $\Delta E_{(1b1-3s)}$; $A^1B_1$ | | 6.90 | 6.51 | | | | | | | 6.67$^q$ |
| $\Delta E_{(1b1-3px,y)}$; $D^1A_1$ | 10.27 | 10.21 | | | | | | | 10.17$^q$ | |
| OH | | | | | | | | | | |
| I.P.$^g$ | 11.32 | 12.42 | 12.71 | 12.75 | 12.70 | | 12.38$^s$ | 11.27$^t$ | 11.44$^x$ | 15.759$^A$ |
| | | | | | | 13.36$^u$ | 15.53$^y$ | | | |
| E.A.$^r$ | 1.54 | 1.73 | 1.81 | 1.91 | 1.85 | | 1.48$^s$ | 1.91$^v$ | 5.652$^y$ | 1.83$^B$ |
| $\Delta E_{(X2\Pi-A2\Sigma+)}$ | 3.98 | 4.11 | | | | 3.95$^s$ | 4.17$^w$ | 4.0$^z$ | 4.05$^C$ | |
| $\Delta E_{(X2\Pi-4\Sigma-)}$ | | 7.04 | 7.33 | | | | | 7.65$^w$ | 6.9$^z$ | |
| $\Delta E_{(X2\Pi-2\Sigma-)}$ | | 7.96 | 8.28 | | | | | 8.51$^w$ | 7.9$^z$ | |
| $\Delta E_{(X2\Pi-2\Delta)}$ | 9.87 | 10.16 | | | | | 10.37$^w$ | 9.9$^z$ | | |
| $\Delta E_{(X2\Pi-2\Pi)}$ | 10.48 | 10.75 | | | | | | 10.6$^z$ | | |
| $\Delta E_{(X2\Pi-4\Pi)}$ | 10.49 | 10.77 | | | | | 11.09$^w$ | 10.6$^z$ | | |
| $\Delta E_{(X2\Pi-2\Sigma+)}$ | | 11.87 | 11.52 | | | | | 11.31$^w$ | 11.50$^z$ | |

**(continued Table IV)**

| | HF | SECI[a] | SDCI[a] | MP2[b] | CCSD(t)[b] | HF[c] | CI[d] | CEPA[e] | exptl |
|---|---|---|---|---|---|---|---|---|---|
| $H_2$ | | | | | | | | | |
| I.P.[g] | 14.52 | 15.21 | 15.43 | 15.25 | 15.46 | 15.43 | 14.55[t] | | 13.36[x] |
| E.A.[r] | 1.26 | 1.33 | 1.38 | 1.35 | 1.39 | 1.48 | | | 1.38[x] |

[a] SECI and SDCI energies were obtained with the MOs and geometries of $H_3O^+$ calculated by RHF at each internuclear distance. [b] Values were obtained with Gaussian 98. [c] Reference 44. [d] Reference 46. [e] Reference 49. [f] Potential energy gaps between each states on the surface of $H_3O$ dissociating ($OH + H_2$). [g] Ionization potential energies of $H_3O$, $H_2O$, OH, and $H_2$. [h] Reference 47. [i] Reference 43. [j] Reference 37. [k] Reference 40. [l] Reference 10. [m] Electronic energy difference between $H_2O$ and $H_3O^+$. [n] Reference 82. [o] Reference 83. [p] Reference 84. [q] Reference 85. [r] Electron affinity of OH and $H_2$. [s] Reference 86. [t] Reference 87. [u] Cited from Reference 88. [v] Reference 89. [w] Reference 90. [x] Reference 88. [y] Reference 91. [z] Reference 92. [A] Reference 93. [B] Reference 94. [C] Reference 95.

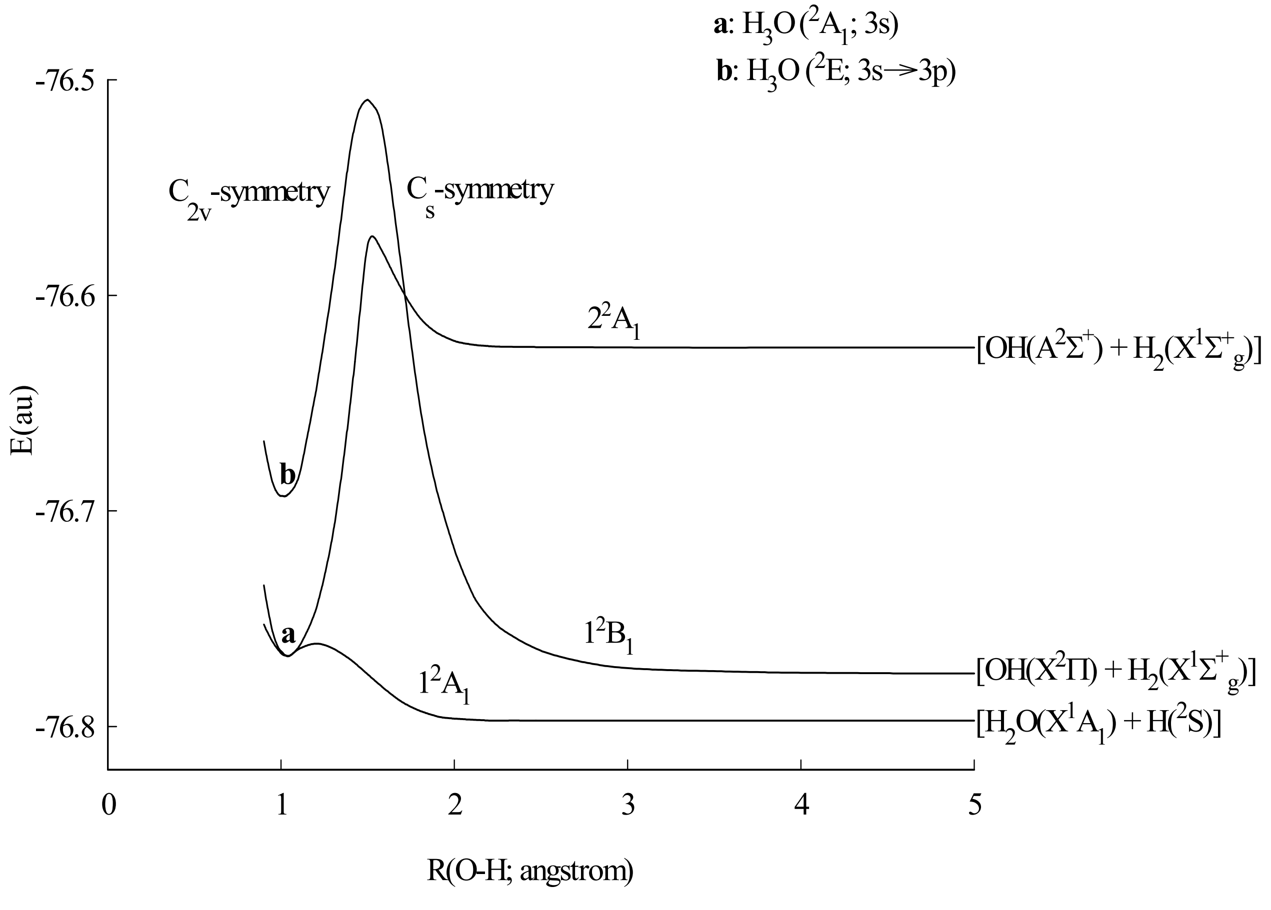

Figure 5. Potential energy curves for the $^2A_1$ and $^2B_1$ states of the Rydberg $H_3O$ radical dissociating into ($H_2O$ + H) and (OH + $H_2$) obtained with the SDCI level.

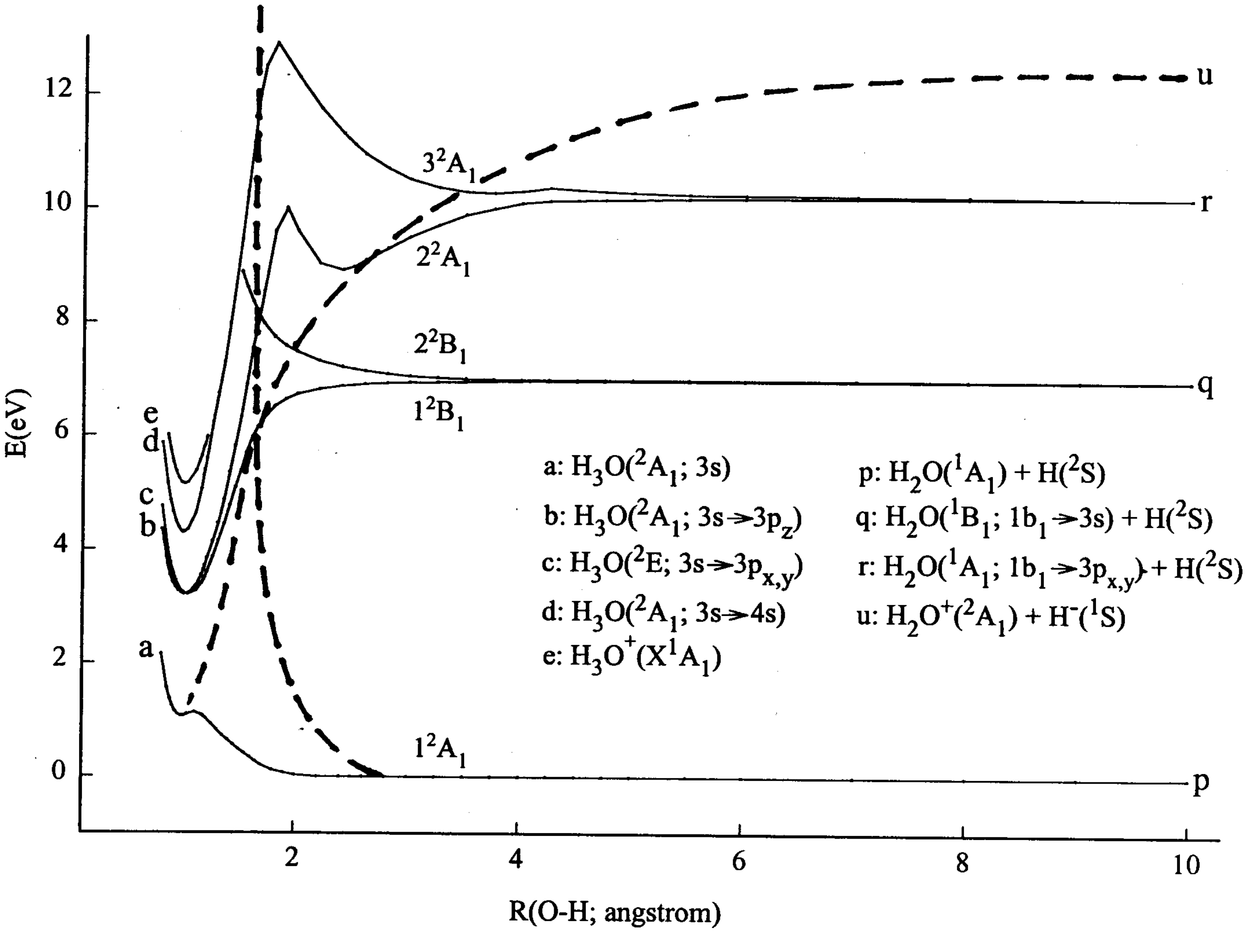

Figure 6. Adiabatic potential energy curves for the ground and excited states of the Rydberg $H_3O$ radical dissociating into ($H_2O$ + H). Broken lines indicate estimated diabatic potential curves.

**Table V.** Contributions of the dominant configuration for the low lying Rydberg $^2A_1$ states along the $H_3O$ radical dissociating into ($H_2O$ + H). 22221 denotes $2a_1^2$ $1e^4$ $3a_1^2$ $4a_1^1$ configuration. The core part is abbreviated and a degenerated orbital of $1e^4$ is indicated as 22.

| $R_{(OH)}$(Å) | $1^2A_1$ | | $2^2A_1$ | | $3^2A_1$ | |
|---|---|---|---|---|---|---|
| 0.8 | 22221 | 0.9982 | 22220010 | 0.9989 | 222200010 | 0.9997 |
| 0.9 | 22221 | 0.9970 | 22220010 | 0.9976 | 222200010 | 0.9990 |
| 1.0 | 22221 | 0.9957 | 22220010 | 0.9959 | 222200010 | 0.9987 |
| 1.2 | 22221 | 0.9924 | 22220010 | 0.9924 | 222200100 | 0.9972 |
| 1.4 | 22221 | 0.9893 | 22220010 | 0.9827 | 222200100 | 0.9914 |
| 1.6 | 22221 | 0.9800 | 22220010 | 0.9681 | 222200100 | 0.9837 |
| 1.8 | 22221 | 0.9819 | 22220010 | 0.9322 | 222200100 | 0.9261 |
| 2.0 | 22221 | 0.9838 | 22220010 | 0.8301 | 222110100 | 0.7155 |
| 2.2 | 22221 | 0.9851 | 22210002 | 0.4418 | 222110001 | 0.6599 |
| | | | 22220010 | 0.2301 | | |
| 2.5 | 22221 | 0.9864 | 22210002 | 0.4875 | 222110001 | 0.6856 |
| | | | 22220010 | 0.2801 | | |
| 3.0 | 22221 | 0.9873 | 22210002 | 0.5046 | 222110001 | 0.7009 |
| | | | 22211001 | 0.3236 | | |
| 3.5 | 22221 | 0.9886 | 22210002 | 0.5375 | 222110001 | 0.6714 |
| | | | 22211001 | 0.4036 | | |
| 4.0 | 22221 | 0.9890 | 22210002 | 0.6009 | 222100002 | 0.7009 |
| | | | 22211001 | 0.4460 | | |
| 5.0 | 22221 | 0.9893 | 22211001 | 0.4915 | 222110001 | 0.5805 |
| 6.0 | 22221 | 0.9896 | 22211001 | 0.5458 | 222110001 | 0.6164 |
| 7.0 | 22221 | 0.9898 | 22211001 | 0.5609 | 222110001 | 0.6865 |
| 8.0 | 22221 | 0.9990 | 22211001 | 0.5720 | 222110001 | 0.6923 |
| 10.0 | 22221 | 0.9993 | 22211001 | 0.5817 | 222110001 | 0.7715 |

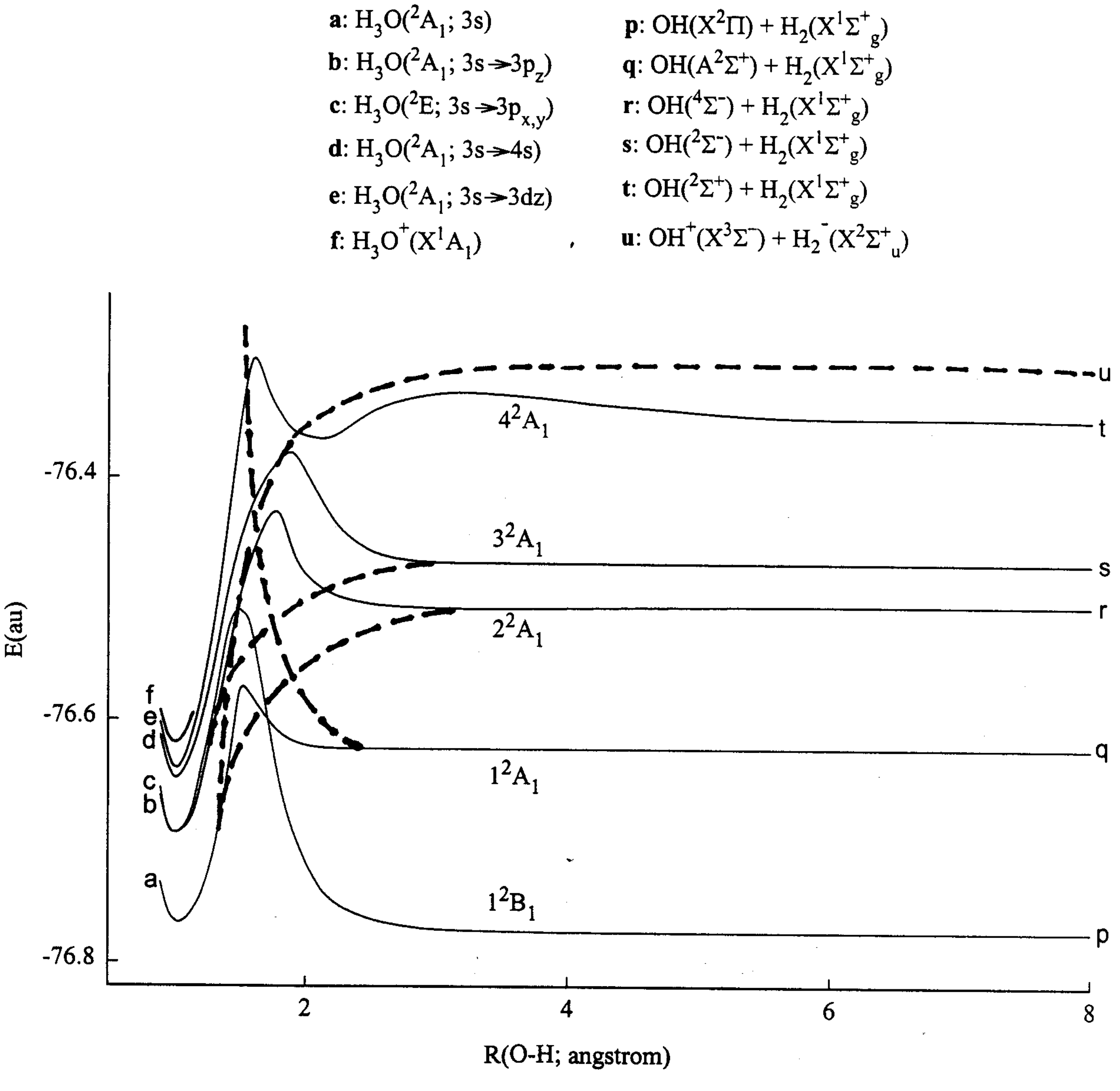

Figure 7. Avoided curve crossings for the $^2A_1$states of the Rydberg $H_3O$ radical dissociating into ($OH + H_2$). Broken lines indicate estimated diabatic potential curves.

**TABLE VI.** Contributions of the dominant configuration for two $^2A_1$ states along the $H_3O$ radical dissociating into ($OH + H_2$). Configuration of $2a_1^2\ 1e^4\ 3a_1^2\ 4a_1^1$ denotes 2421. The core part is abbreviated.

| $R_{(OH)}$ (Å ) | $1^2A_1$ | | $2^2A_1$ | |
|---|---|---|---|---|
| 0.8 | 242100 | 0.9951 | 24200001 | 0.9596 |
| 0.9 | 242100 | 0.9922 | 24200001 | 0.9486 |
| 1.0 | 242100 | 0.9892 | 24200001 | 0.9379 |
| 1.1 | 242100 | 0.9821 | 24200001 | 0.9185 |
| 1.2 | 222210 | 0.9736 | 22112001 | 0.8951 |
| 1.4 | 222210 | 0.8967 | 22112001 | 0.7825 |
| 1.5 | 222210 | 0.7749 | 22112001 | 0.5976 |
| | | | 22110021 | 0.3858 |
| 1.6 | 222201 | 0.6879 | 22211001 | 0.4786 |
| | | | 22110021 | 0.5053 |
| 1.8 | 222201 | 0.6709 | 22211001 | 0.3520 |
| | | | 22110021 | 0.6472 |
| 2.0 | 212202 | 0.7842 | 22211001 | 0.2308 |
| | | | 22110021 | 0.7354 |
| 2.1 | 212202 | 0.8401 | 22111002 | 0.5650 |
| 2.2 | 212202 | 0.9083 | 22111002 | 0.5916 |
| 2.3 | 212202 | 0.9187 | 22111002 | 0.6447 |
| 2.5 | 212202 | 0.9241 | 22111002 | 0.6772 |
| 3.0 | 212202 | 0.9329 | 22111002 | 0.7270 |
| 3.5 | 212202 | 0.9381 | 22111002 | 0.7973 |
| 4.0 | 212202 | 0.9416 | 22111002 | 0.8377 |
| 5.0 | 212202 | 0.9426 | 22111002 | 0.8539 |
| 6.0 | 212202 | 0.9434 | 22111002 | 0.8580 |
| 7.0 | 212202 | 0.9442 | 22111002 | 0.8603 |
| 8.0 | 212202 | 0.9446 | 22111002 | 0.8699 |

# 4 CONCLUSIONS

We have calculated the state-to-state correlation curves for the dissociation reaction of the Rydberg $[(AH_a^+)(e^-)_{Rydberg}]$ radical into ($AH_b + H_c$) under the $C_{2v}$- and $C_{3v}$-symmetry constraints and analyzed the contributions of the dominant configurations for the ground and low lying excited states. The ground potential curve has a relatively low potential energy barrier and the maximum position of the potential barrier exists near the equilibrium geometry of $AH_a$. The potential barriers are formed by two kinds of the avoided curve crossings. One is occurred between the dissociative diabatic states emerging from $[(AH_a^+)(e^-)_{Rydberg}]$ and the repulsive diabatic states from an antibonding interaction of $[AH_b^*(n\rightarrow 3s) + H_c]$. At shorter than $R_{(AH)}\cong 2.0$ Å, the curve crossing are represented mainly. The other is occurred between the repulsive diabatic states emerging from $[AH_b^*(n\rightarrow 3s) + H_c]$ and the attractively ionic diabatic states from the $[AH_b^+ + H_c^-]$ asymptotes. The curve crossings are also represented at larger than $R_{(AH)}\cong 2.0$ Å. When $AH^+$ and $H_2^-$ ions approach to each other from infinite separation, there exists strong electrostatic attraction between two ions. The attractive state state emerging from the cation-anion pair is bound strongly. These curve crossings are greatly influenced by the attractive characters from the cation-anion pair $[AH_b^+ + H_c^-]$ asymptote. In the excited curves, the potential energy curves are also shallowly bound. The potential wells are also formed by the avoided curve crossings between the dissociative diabatic excited states of $[(AH_a^+)(e^-)_{Rydberg}]$ and the repulsive diabatic states from the antibonding interactions of $[AH_b^*(n\rightarrow 3s) + H_c]$.

In $AH_a$ dissociating into ($AH_b$ + $H_c$), each state of $AH_a$ corresponds to each state emerging from ($AH_b$ + $H_c$). In the correlation curve if the potential energy barriers of the states are determined by the avoided curve crossings, the barrier height should be high and the maximum position should be located at middle place between $[(AH_a^+)(e^-)_{Rydberg}]$ and ($AH_b$ + $H_c$). But, the potential barrier heights of the excited states are appeared to be low and the barriers are located near the equilibrium geometry of $AH_a$. In $[(AH_a^+)(e^-)_{Rydberg}]$ dissociating into ($AH_b^+$ + $H_c^-$), this state is diabatically bound due to the strongly cation-anion electrostatic attraction. As the result, the position of the avoided curve crossing is shifted to the equilibrium geometry of $[(AH_a^+)(e^-)_{Rydberg}]$ and the maximum position of potential barrier of the ground state formed by the avoided curve crossing is located out of line of those of the excited potential energy curves. The attractive diabatic characters emerging from ($AH_b^+$ + $H_c^-$) may be played an important role in the state-to-state correlation curves for the dissociation reaction.

For $NH_4$ dissociating into ($NH_3$ + H), the energy barrier height of $^2A_1$ from the transition state to $NH_4$ is ≅0.83 eV. For $NH_4$ dissociating into ($NH_2$ + $H_2$), The barrier heights of $^2A_1$ and $^2B_1$ from the transition state to $NH_4$ are ≅3.59 and 2.96 eV, respectively. For the $^2A_1$ state of $H_3O$ dissociating into ($H_2O$ + H), the energy difference from the transition state to $H_3O$ is ≅0.12 eV. In $H_3O$ dissociating into (OH + $H_2$), the energy differences of the $^2A_1$ and $^2B_1$ states from the transition state to $H_3O$ are ≅4.99 and ≅5.02 eV, respectively. Because the equilibrium geometric structure of $H_2F$ have not been optimized, the potential barriers for $H_2F$ dissociating into its asymptotes are nearly zero. Therefore, along the A-H bond rupture, the ground states of $NH_4$, $H_3O$, and $H_2F$ have energy barriers of ≅0.83, 0.12, and 0 eV, respectively. The relative potential barriers from $NH_4$ to $H_2F$ decrease stepwise. Because the relative potential barrier of $NH_4$ is largest than those of $H_3O$ and $H_2F$, the existence of $NH_4$ in cluster has been observed experimentally. But, $H_3O$ and $H_2F$ have been scarcely observed.

### Acknowledgment

We thank the Korea Research Foundation (KRF) for supporting this work through the Basic Science Research Institute program (KRF-2002-015-CP0161). The author thanks Dr. Hosung Sun for valuable helps.

**Keywords**. Rydberg radical, potential energy curve, avoided curve crossing, diabatic state, adiabatic state, asymptote, metastable state, configuration interaction, potential well, potential energy gap

## 5 REFERENCES

[1] F. Misaizu, P. L. Houston, N. Nishi, H. Shinohara, T. Kondow, and K. Kinoshita,. *J. Chem. Phys*., **1993**, *98*, 336.
[2] L. A. Posey, R. D. Guettler, N. J. Kirchner, and R. N. Zare, *J. Chem. Phys*., **1994**, *101*, 3772.
[3] S. A. Buzza, S. Wei, J. Purnell, and A. W. Castleman, Jr., *J. Chem. Phys*., **1995**, *102*, 4832.
[4] F. Fuke, R. Takasu, and F. Misaizu, *Chem. Phys. Lett*., **1994**, 229, 597; K. Fuke, and R. Takasu, *Bull. Chem. Soc. Jpn*., **1995**, *68*, 3309.
[5] G. Herzberg, *Faraday Discuss. Chem. Soc*., **1981**, *71*, 165.
[6] O. S. Mortensen, B. R. Henry, and M. A. Mohammadi, *J. Chem. Phys*., **1981**, *75*, 4800.
[7] S. T. Ceyer, P. W. Tiedemann, B. H. Mahan, and Y. T. Lee, *J. Chem. Phys*., **1979**, *70*, 14.
[8] A. Schuster, *Rep. Brit. Assoc*., 1872, pp.38.
[9] H. Schüler, A. Michel, and A. E. Grün, *Z. Naturforsch*., **1955**, *10a*, 1.
[10] B. W. Williams and R. F. Porter, *J. Chem. Phys*., **1980**, *73*, 5598.
[11] G. I. Gellene, D. A. Cleary, and R. F. Porter, *J. Chem. Phys*., **1983**, *77*, 3471.
[12] G. Herzberg and J. T. Hougen, *J. Mol. Spectrosc*., **1983**, *97*, 430.
[13] E. A. Whittaker, B. J. Sullivan, G. C. Bjorklund, H. R. Wendt, and H. E. Hunziker, *J. Chem. Phys*., **1984**, *80*, 961.
[14] J. K. G. Watson, *J. Mol. Spectrosc*., **1984**, *103*, 125; *J. Mol. Spectrosc*., **1984**, *107*, 124.

[15] F. Alberti, K. P. Huber, and J. K. G. Watson, *J. Mol. Spectrosc*., **1984**, *107*, 133.
[16] R. Signorell, H. Palm, and F. Merkt, *J. Chem. Phys*., **1997**, *106*, 6523.
[17] F. Misaizu, K. Tsukamoto, M. Sanekata, and K. Fuke, *Chem. Phys. Lett*., **1992**, *188*, 241.
[18] I. V. Hertel, C. Hüglin, C. Nitsch, and C. P. Schultz, *Phys. Rev. Lett*., **1991**, *67*, 1767.
[19] E. Kariv-Miller, C. Nanjundiah, J. Eaton, and K. E. Swenson, *J. Electroanal. Chem*., **1984**, *167*, 141.
[20] J. K. Park, *J. Chem. Phys*., **1997**, *107*, 6795; J. K. Park, *J. Chem. Phys*., **1998**, *109*, 9753.
[21] E. M. Evleth and E. Kassab, *Pure Appl. Chem*., **1988**, *60*, 209.
[22] E. Kassab and E. M. Evleth, *J. Am. Chem. Soc*., **1987**, *109*, 1653.
[23] J. Kaspar, V. H. Smith, Jr., and B.N. McMaster, *Chem. Phys*., **1985**, *96*, 81.
[24] M. Meot-Ner, *J. Am. Chem. Soc*., **1984**, *106*, 1257.
[25] H. Cardy, D. Liotard, A. Dargelos, and E. Poquet, *Chem. Phys*., **1983**, *77*, 287.
[26] S. Havriliak and H. F. King, *J. Am. Chem. Soc*., **1983**, *105*, 4.
[27] E. Broclawik, J. Mrozek, and V. H. Smith, Jr., *Chem. Phys*., **1982**, *66*, 417.
[28] D. L. Albritton, *At. Data Nucl. Data*, **1978**, *Tables 22*, 1.
[29] A. Pullman and A. M. Armbruster, *Chem. Phys. Lett*., **1975**, *36*, 558.
[30] W. A. Lathan, W. J. Hehre, L. A. Curtiss, and J. A. Pople, *J. Am. Chem. Soc*., **1971**, *93*, 6377.
[31] W. Strehl, H. Hartmann, K. Hensen, and W. Sarholz, *Theo. Chim. Acta*, **1970**, *18*, 290.
[32] R. S. Mulliken, *J. Chem. Phys*., **1933**, *1*, 492.
[33] H. J. Bernstein, *J. Am. Chem. Soc*., **1963**, *85*, 484.
[34] J. L. Magee, *Radiat. Res. Suppl*., **1964**, *4*, 20.
[35] T. J. Sworski, *J. Am. Chem. Soc*., **1964**, *86*, 5034; *J. Am. Chem. Soc*., **1955**, *77*, 4689.
[36] M. Kongshaug, H. B. Steen, and B. Cercek, *Nature Phys. Sci*., **1971**, *234*, 97.
[37] C. E. Melton and H. W. Joy, *J. Chem. Phys*., **1967**, *46*, 4275; *J. Chem. Phys*., **1968**, *48*, 5286.
[38] T. W. Martin and L. L. Swift, *J. Am. Chem. Soc*., **1971**, *93*, 2788.
[39] T. A. Claxton, I. S. Ginns, M. J. Godfrey, K. V. S. Rao, and M. C. R. Symons, *J. Chem. Soc. Faraday Trans. II*, 1973, *69*, 217.
[40] G. I. Gellene and R. F. Porter, *J. Chem. Phys*., **1984**, *81*, 5570.
[41] B. E. Turner, *Symp. Int. Astron. Union*, **1992**, *150*, 181.
[42] D. Bassi, M. De Paz, A. Pesce, and F. Tommasini, *Chem. Phys. Lett*., **1974**, *26*, 422.
[43] D. M. Bishop, *J. Chem. Phys*., **1968**, *48*, 5285.
[44] R. A. Gangi and R. F. W. Bader, *Chem. Phys. Lett*., **1971**, *11*, 216.
[45] W. A. Lathan, W. J. Hehre, L. A. Curtiss, and J. A. Pople, *J. Am. Chem. Soc*., **1971**, *93*, 6377.
[46] K. S. E. Niblaeus, B. O. Roos, and P. E. M. Siegbahn, *Chem. Phys*., **1977**, *25*, 207.
[47] S. Raynor and D. R. Herschbach, *J. Phys. Chem*., **1982**, *86*, 3592.
[48] I. Martin, P. Campo, and C. Lavin, *Int. J. Quantum Chem. Symp*., **1995**, *29*, 631.
[49] M. Luo and M. Jungen, *Chem. Phys. Lett*., **1999**, *241*, 297.
[50] M. E. Schwarz, *Chem. Phys. Lett*., **1976**, *40*, 1.
[51] J. K. Park, *Chem. Phys. Lett*., **1999**, *315*, 119; *Chem. Phys. Lett*., **2002**, *356*, 63.
[52] W. R. Wadt and N. W. Winter, *J. Chem. Phys*., **1977**, *67*, 3068.
[53] A. Mavridis and J. F. Harrison, *J. Chem. Soc. Faraday Trans*., **1982**, *78*, 447.
[54] M. Bettendorff, R. J. Buenker, S. D. Peyerimhoff, and J. Römelt, *Z. Phys. A,* **1982**, *304*, 125.
[55] P. Botschwina, in Molecular Ions: Geometrical and Electronic Structures, edited by J. Berkowitz and K. Groeneveld, Plenum, New York, 1983.
[56] H. F. Schaefer III, *J. Phys, Chem*., **1985**, *89*, 5336.
[57] J. C. Polanyi, M. G. Prisant, and J. S. Wright, *J. Phys, Chem*., **1987**, *91*, 4727.
[58] I. D. Petsalakis, G. Theodorakopoulos, J. S. Wright, and I. P. Hamilton, *J. Chem. Phys*., **1988**, *88*. 7633.
[59] I. D. Petsalakis, G. Theodorakopoulos, J. S. Wright, and I. P. Hamilton, *J. Chem. Phys*., **1988**, *89*. 6841.
[60] M. Gutowski and J. Simons, *J. Chem. Phys*., **1990**, *93*, 2546.
[61] F. Chen and E. R. Davidson, *J. Phys, Chem*., **2001**, *105*, 10915.
[62] M. J. Frisch, J. S. Binkley, and H. F. Schaefer III, *J. Chem. Phys*., **1984**, *81*, 1882.
[63] A. B. Raksit, S.-J. Jeon, and R. F. Porter, *J. Phys, Chem*., **1986**, *90*, 2298.
[64] E. Schäfer and R. J. Saykally, *J. Chem. Phys*., **1984**, *81*, 4189.
[65] S. Huzinaga, J. Andzelm, M. Klobukowski, E. Radzio-Andzelm, Y. Sakai, and H. Tatewaki, *Physical Science Data*, Gaussian basis sets for molecular calculations, Vol. 16, Elsevier, Amsterdam, 1984.
[66] F. B. Duijneveldt, *IBM Research Report NO. R J*, **1971**, 945.
[67] K. Hasimoto and Y. Osamura, *J. Chem. Phys*., **1991**, *95*, 1121.
[68] H. Partridge, C. W. Bauschlicher, Jr., and S. R. Langhoff, *Theo. Chim. Acta*, **1990**, *77*, 323.
[69] R. Poirier, R. Kari, and I. G. Csizmadia, *Physical Science Data*, Handbook of Gaussian basis sets, Vol. 24, Elsevier, Amsterdam, 1984.

[70] A. Skerbele and E. N. Lassettre, *J. Chem. Phys*., **1965**, *42*, 395.
[71] D. H. Aue and M. T. Bowers, *Gas Phase Ion Chemistry II*, Eds. M. T. Bowers, Academic Press, New York, 1979, pp.1.
[72] R. Runau, S. D. Peyerimhoff, and R. J. Buenker, *J. Mol. Spectrosc*., **1977**, *68*, 253.
[73] R. L. Graham, J. T. Golab, and D. L. Yeager, *J. Chem. Phys*., **1988**, *88*, 2572.
[74] J. A. Pople and L. A. Curtis, *J. Phys. Chem*. **1987**, *91*, 155.
[75] S. J. Dunlavey, J. N. Dyke, N. Jonathan, and A. Morris, *Mol. Phys*., **1980**, *39*, 1121; J. N. Dyke, N. Jonathan, and A. Morris, *Int. Rev. Phys. Chem*., **1982**, *2*, 3.
[76] S. A. Pope, I. H. Hillier, and M. J. Guest, *Faraday Symp. Chem. Soc*., **1984**, *19*, 109.
[77] S. T. Gibson, J. P. Greene, and J. Berkowitz, *J. Chem. Phys*., **1985**, *83*, 4319.
[78] R. Vetter, L. Zülicke, A. Koch, E. F. van Dishoeck, and S. D. Peyerimhoff, *J. Chem. Phys*., **1996**, *104*, 5558.
[79] H. Biehl, G. Schönnenbeck, F. Stuhl, and V. Staemmler, *J. Chem. Phys*., **1994**, *101*, 3819.
[80] R. P. Saxon, B. H. Lengsfield III, and B. Liu, *J. Chem. Phys*., **1983**, *78*, 312.
[81] S. D. Peyerimhoff and R. J. Buenker, *Can. J. Chem*., **1979**, *57*, 3182.
[82] L. A. Curtiss, K. Raghavachari, G. W. Trucks, and J. A. Pople, *J. Phys. Chem*., **1991**, *94*, 7221.
[83] H. H. Bueker and E. Uggerud, *J. Phys. Chem*., **1995**, *99*, 5945.
[84] C. Y. Ng, D. J. Trevor, P. W. Tiedemann, S. T. Ceyer, P. L. Kronebusch, B. H. Mahan, and Y. T. Lee, *J. Phys. Chem*., **1977**, *67*, 4235.
[85] G. Herzberg, *Moleclar Spectra and Moleclar Structure III*. Electronic Spectra and Electronic Structure of Polyatomic Molecules, Van Nostrand, New York, 1966.
[86] H. Sun, M. G. Sheppard, and K. F. Freed, *J. Chem. Phys*. **1981**, *74*, 6842.
[87] A. Streitwieser, Jr. and R. W. Taft, *Progress in Physical Organic Chemistry*, **1974**, *11*, 175.
[88] P. E. Cade and W. M. Huo, *J. Chem. Phys*., **1967**, *47*, 614.
[89] P. E. Cade, *Proc. Phys. Soc*., **1967**, *91*, 842.
[90] R. D. Vivie, C. M. Marian, and S. D. Peyerimhoff, *Mol. Phys*., **1988**, *63*, 3.
[91] A. D. Esposti and H.-J.Werner, *J. Chem. Phys*., **1990**, *93*, 3351.
[92] P. J. Bruna, G. Hirsch, R. J. Buenker, and S. D. Peyerimhoff, *Molecular Ions, NATO, ASI Series*, 1984, pp. 309.
[93] G. Herzberg, *Molecular Spectra and Molecular Structure IV,* Constants of Diatomic Molecules; Spectra of Diatomic Molecules, Van Nostrand Reinhold, New York, 1979.
[94] E. de Beer, E. H. Kim, D. M. Neumark, R. F. Gunion, and W. C. Lineberger, *J. Phys. Chem*. **1995**, *99*, 13627.
[95] R. L. Kelly and D. E. Harrison, Jr., *Atomic Data*, **1971**, *3*, 177.

## Biographies

**Author** is assistant professor of chemistry at the Pusan National University. After obtaining a Ph.D. degree in physical chemistry of “Applications of Effective Valence Shell Hamiltonian to the Valence States of NH, SiH, PH, and SH” from the Pusan National University, Dr. Park undertook postdoctoral research with Professor Iwata at Institute of Molecular Science. More recently, Dr. Park has collaborated on projects with Professor Lee at Pusan National University.